CHALMERS
UNIVERSITY OF TECHNOLOGY

Precision Manufacturing of Radio Frequency Microwave Filter Structures Using Additive Manufacturing Technologies

An investigation of the Additive Manufacturing techniques Metal Binder Jetting, and Laser Powder Bed Fusion for manufacturing Radio Frequency Filters for Microwave radio links and Base stations

Master's Thesis in MSc Production Engineering

NISHANT PATTANAIK
PRAJWAL SRINIVAS

DEPARTMENT OF INDUSTRIAL AND MATERIAL SCIENCE
CHALMERS UNIVERSITY OF TECHNOLOGY
Gothenburg, Sweden 2025
www.chalmers.se

Master's thesis 2025

Precision Manufacturing of Radio Frequency Microwave filter structures using Additive Manufacturing Technologies

An investigation of the Additive Manufacturing techniques Metal Binder Jetting, and Laser Powder Bed Fusion for manufacturing Radio Frequency Filters for Microwave Radio Links and Base stations.

NISHANT PATTANAIK

PRAJWAL SRINIVAS

CHALMERS
UNIVERSITY OF TECHNOLOGY

Department of Industrial Materials and Science
Division of Production Engineering
Chalmers University of Technology
Gothenburg, Sweden 2025

Precision Manufacturing of Radio Frequency Microwave filter structures using Additive Manufacturing Technologies
An investigation of the Additive Manufacturing techniques Binder Jetting, and Laser Powder Bed Fusion for manufacturing Radio Frequency Filters for Microwave Radio Links and Base stations.
NISHANT PATTANAIK

PRAJWAL SRINIVAS

Examiner: Lars Nyborg, Department of Industrial and Material Science
Academic Supervisor: Erika Tuneskog
Supervisor: Torbjörn Westin, Ericsson

Master's Thesis 2025
Department of Industrial and Material Science
Division of Materials and Manufacturing
Chalmers University of Technology
SE-412 96 Gothenburg
Telephone +46 31 772 1000

Cover: Precision Manufacturing of Radio Frequency Microwave filter structures using Additive Manufacturing Technologies.

Typeset in LaTeX
Printed by Chalmers Reproservice
Gothenburg, Sweden 2025

Precision Manufacturing of Radio Frequency Microwave filter structures using Additive Manufacturing Technologies.
An investigation of the Additive Manufacturing techniques Metal Binder Jetting, and Laser Powder Bed Fusion for manufacturing Radio Frequency Filters for Microwave Radio Links and Base stations.
NISHANT PATTANAIK
PRAJWAL SRINIVAS
Department of Industrial and Material Science
Chalmers University of Technology

Abstract

There is a growing demand for high-speed communication, to enable this high frequency transmission links are utilized. These links employ microwave radio frequency waveguide filters. Conventional manufacturing of the filters face limitations in producing multi-cavity structures with complex geometries. Additive manufacturing processes offer design freedom, reduced material wastage and rapid prototyping, making it an alternative to produce these filters.

This study investigates the feasibility to manufacture the waveguide filters with the frequencies E-Band (65 - 67 GHz) and D-Band (130 - 135 GHz) using two metal Additive manufacturing processes, Binder Jetting Technology (BJT) and Powder Bed Fusion - Laser Beam (PBF-LB). The filters were manufactured using a Markforged PX100™ BJT printer by Bosch GmbH and an EOS M100 PBF-LB printer at Chalmers University of Technology. The BJT filters were printed in two phases, the first was a trial phase to determine the surface roughness measurements that were done on selected surfaces of the parts to determine a suitable orientation for the final print. In the second and final phase, a total of 40 filters were printed, 20 for each band. For PBF-LB, 10 parts were printed 5 for each band. All 40 BJT and 6 PBF-LB filters underwent electrical characterization using a Vector Network Analyzer. Five BJT filters of each frequency bands that reached near-target passband frequency and low loss magnitude were selected for surface treatment with electroless copper plating to improve performance.

Results showed that BJT-manufactured E-Band filters achieved insertion losses within the target range while maintaining the required passband frequency, whereas a subset of D-Band BJT filters met the desired specifications. PBF-LB-manufactured filters resulted in higher losses and dimensional inaccuracies due to deviations in internal geometry. The loss magnitudes were reduced by copper plating by nearly half for both E-Band and D-Band filters. Overall, BJT demonstrated greater suitability to manufacture high-frequency waveguide filters.

Acknowledgements

This master's thesis was carried out in cooperation with the Mechanical and Thermal Design Department at Ericsson AB in Lindholmen, Gothenburg, and Chalmers University of Technology. We thank both institutions for giving us the opportunity and resources to complete this project.

We would like to take this opportunity to express our sincere gratitude to our academic supervisor, Erika Tuneskog, for her continuous motivation and support during the project period. We also thank our examiner, Professor Lars Nyborg, for his assistance and support.

We thank our industrial project supervisor at Ericsson, Torbjörn Westin, for his guidance, support, and encouragement during the project. We would like to thank Klass Erikson, Senior Researcher at Ericsson, for his helpful technical support and cooperation. We appreciate Thanh Do and Thomas Emanuelsson from the Electrical Department for their collaboration and contribution. We acknowledge the efforts put in by Gilbert Johansson in helping us with component splitting. We want to thank Tony Josefson at Ericsson in Borås for his assistance with the surface measurements and dimensional analysis of the components, which was very important to our study. We also thank Provexa for their work on conducting surface treatments on the manufactured components. We appreciate Bosch's cooperation as our component supplier during the project.

Finally, we would like to thank our families and friends for their unwavering support throughout this thesis project.

Nishant Pattanaik
Prajwal Srinivas
Gothenburg, 2025

List of Acronyms

Below is the list of acronyms that have been used throughout this thesis listed in alphabetical order:

AM	Additive Manufacturing
BJT	Binder Jetting Technology
DED	Direct Energy Deposition
DFAM	Design For Additive Manufacturing
LMM	Lithography-based Metal Manufacturing
MJT	Material Jetting Technology
PBF-LB	Powder-Bed Fusion Technology - Laser Beam
RF	Radio Frequency
EDM	Electrical Discharge Machining
ECP	Electroless Copper Plating

Contents

List of Figures

List of Tables

1

Introduction

1.1 Background

Ericsson is a world leader in the rapidly changing environment of communications technology. This research is conducted in cooperation with Ericsson in the department of "Mechanical and Thermal Design" under the hardware unit and Chalmers University of Technology.

With increasing demand for mobile data, communication networks such as 5G and emerging 6G systems are driving the need for highly integrated, miniaturized, and high-performance Radio frequency filters. The Ericsson Mini-Link 6000 series is a microwave radio system, offering high capacity, flexibility, and cost-effectiveness for mobile transport networks [3]. A radio frequency filter lets a specific band of frequencies pass through and restricts others [4]. Waveguide filters are RF filters capable of carrying signals at high frequencies with a low loss in microwave and millimeter wave bandwidths [5]. This filter is used in most high-frequency communications systems, including radar, satellite communications, and cellular networks. [6][7]. This thesis would deal with waveguide RF filters of the E-band and D-band, which would be of great interest to Ericsson. E-band operates at a range of 60-90 GHz, and D-Band operates at 110-170 GHz[8]. These bands are critical for Ericsson's network evolution plans. Ericsson predicts that by 2027, E-Band adoption could reach 25% of new deployments [9]. E-band being already used in 5G communication and D-band could potentially be useful during future 6G implementation [9].

Conventional manufacturing techniques face major limitations in producing compact, multi-cavity filters with complex internal geometries at millimeter-wave frequencies. The development of Additive Manufacturing (AM) technologies can significantly contribute to the advancement of high-frequency filters in microwave radio devices. Given the design and dimensional freedom, reduced material wastage, and faster prototyping, Ericsson is exploring the Additive manufacturing option for manufacturing this new critical part. Since 2019, Ericsson has been involved in AM research and hopes to one day move from batch production to mass production by using AM, also adhering to sustainable practices. [10].

1.2 Aim

The thesis aims to conduct a feasibility study, investigating which AM technologies are suitable for the RF components with frequencies 65- 67 GHz and 130-134 GHz to support the electrical requirements of high-frequency systems, and to evaluate and analyze how post-treatment influences the performance of the filters.

1.3 Objectives

The focus of the project is to explore feasible AM technology that allows the manufacturing of high-frequency waveguide RF filters. To evaluate AM surfaces and dimensions that have lower insertion loss and achieve the desired frequency output.

The research questions (RQ) formulated from the aim of this thesis are:

- RQ 1. Which AM technologies are most suitable for producing Radio Frequency waveguide filter structures?
- RQ 2. How do post-treatment impact the electrical performance of additively manufactured RF filter structures, and evaluate surface roughness of AM surfaces?
- RQ 3. What design modifications can be implemented to enhance the manufacturability and performance of RF filters and how does dimensional accuracy influence the performance of the filters?

1.4 Limitations

- Supplier restriction from Bosch that the use of copper for printing was not feasible. Copper printing at Chalmers University of Technology using Lithography based Metal Manufacturing (LMM) was also not possible.
- Diamond saw cutting and milling were used to cut the components in different cross-sections, leading to the smeared edges.
- The design of the filter was not optimized from an AM perspective rather from a milling perspective. A single design was used in this thesis work due to the complexity in the design and simulation of the filters.
- The ISO measurement techniques was not feasible as a result of the dimensions of the D-band filters being smaller than required dimensions, especially their reduced cavity and waveguide sizes.

1.5 Delimitations

The study focuses on the design, production, and performance evaluation of waveguide filters fabricated by AM methods, Binder Jetting Technology (BJT), and Powder Bed Fusion - Laser Beam (PBF-LB). The scope is restricted to E-band and D-band frequency ranges alone. Surface roughness measurements for the E-band filters followed ISO standards. Surface plating

is applied only to BJT components made from stainless steel. The research analyzes waveguide filter performance based on simulation and experimental validation, but not by any other validation technique. The material choice is limited to 316L stainless steel. Mechanical test, such as strength tests, was not performed.

1.6 United Nations Sustainable Development Goals (SDG)

This thesis work can potentially address two of the 17 SDGs as outlined by the UN (United Nations Development Program).

SDG 9 Industry, Innovation, and Infrastructure

SDG 9 underscores the resilient infrastructure, emphasizes innovation, and promotes sustainable industrialization. The study contributes to innovation in manufacturing processes by exploring additive manufacturing to produce complex microwave RF products. This work advances SDG 9 by driving innovation and industrial development goals in a sustainable manner.

SDG 12 Responsible Consumption and Production

SDG 12 is centered around the efficient utilization of resources, waste reduction, and the adoption of sustainable practices across the value chains. This project aligns with the goal by utilizing AM processes to manufacture the RF filters, which use less material than the usual conventional methods. Components are built layer by layer in AM processes; therefore, material is being used precisely, and unused powder can be recycled for future builds. This is how the project advances SDG 12 through sustainable manufacturing practices, and reducing environmental impact.

2

Theory

2.1 Waveguide Filters

Waveguide filters are based on the fundamental principle of electromagnetic wave transmission through a waveguide structure. A waveguide is a physical structure that conveys electromagnetic waves between input and output ports, constructed from a conductive material that contains the waves within its bounding edges [7]. A waveguide filter is used in most high-frequency communication systems, including radar, satellite communications and cellular networks. The filters permit some frequencies to pass through and block others, thereby enhancing signal quality and minimizing interference [9],[10].

In waveguide systems operating within the E-band, controlling surface roughness is essential due to the heightened sensitivity of wave propagation to conductor losses. As roughness increases, so does electrical resistance, leading to greater insertion loss and diminished filter efficiency and selectivity [11]. Waveguide components manufactured using an additive manufacturing process have surface roughness values ranging from 10 µm to 50 µm. To mitigate the high surface roughness, several steps have proven effective with post-treatment techniques such as copper infiltration, metal plating [12],[13],[14].

2.1.1 Filter parameters

The performance metrics considered for the filters are insertion loss and return loss, measured using Vector Network Analyzer equipment. The insertion loss is the amount of reduction of signal strength when it passes through a filter, and it is measured in decibels(dB) [15]. The return loss is the amount of signal that is reflected back to the source, measured in decibels (dB) [16]. The VNA displays the scattering parameters S21 and S11, which correspond to the insertion loss and return loss, respectively. In a two port VNA, the signal entering through port 1 and emerging from port 2 is S21 and the signal entering through port 1 and emerging from port 2 is S11 as shown in the figure below [17].

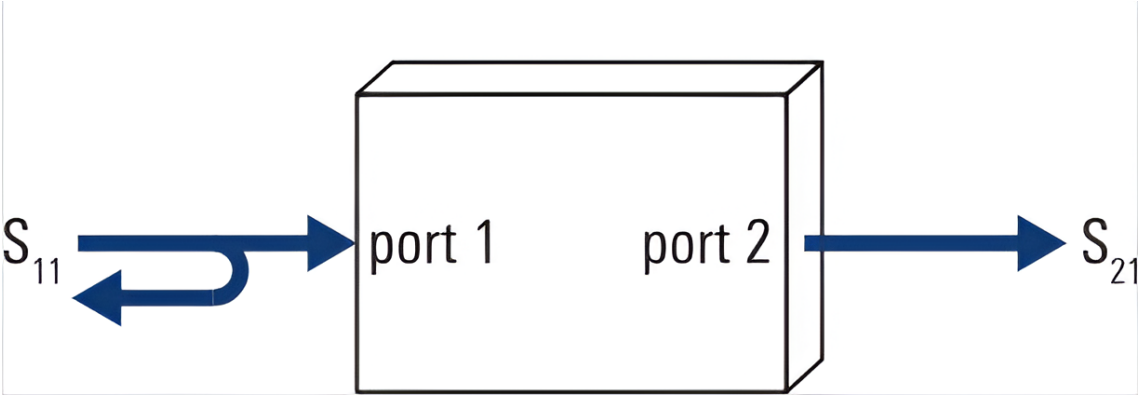

Figure 2.1: S11 and S21.

Another parameter measured using VNA is the frequency Bandwidth. The bandwidth depicts the range of the desired signal frequencies. For Ericsson, the specification of filter parameters would be S11 <-15dB, and S21 being >-0.6dB (E-band) >-1.0 dB (D-band) [18]. Considering the filters manufactured from SS316L, the acceptable S21 magnitude for E-band can be -3 dB, and for D-Band it can be -5 dB[[18]. Furthermore, the number of fluctuations in the S11 curve can correspond to the same number of resonant structures like fins(or irises) within the filter. This can suggest the geometrical accuracy of the manufacturing process [19].
Waveguide filters cover various frequency bands, classified based on the frequencies they permit to pass through and exit [4]. E-band and D-band waveguide filters are higher frequency filters, with the E-band filters having a range of 60 GHz to 90 GHz and D-band filters having a range of 110 GHz to 170 GHz. The filters in the E-band have low insertion loss and narrow bandwidth, while the D-band filters have enhanced design features that help enhance their performance and broaden their bandwidth capacity to be used in future communication technologies such as 6G. The drawbacks of waveguides are that they need precise design and fabrication, as particular dimensions of waveguides are suitable for various frequency ranges [20].

2.2 Additive Manufacturing Techniques

Based on the ASTM definition of AM, it is the process of layer-to-layer joining of material to make components from a 3D model [21]. According to ISO standards [22], AM can be categorized into several processes as described below.

- **Binder Jetting Technology (BJT)** – It is the selective deposition of a liquid binder onto a powder bed to join the powder particles layer by layer.
- **Powder Bed Fusion (PBF)** – In this process, a high-energy source, either a laser beam or an electron beam, is used to selectively fuse regions within a layer of powder.
- **Vat Polymerization (VPP)** – In this AM process, a liquid photopolymer resin contained within a vat is cured selectively using UV. The UV is projected onto a select region to solidify the liquid into the desired shape.
- **Material Jetting Technology (MJT)** – MJT operates by selectively dispensing droplets of build material onto a build platform. This is then cured

using UV or cooled to solidify them into a desired shape.

- **Directed Energy Deposition (DED)** – In this AM technique, a high-energy source like a laser beam, electron beam, or plasma arc is used to melt material as it is being deposited.
- **Material Extrusion (MEX)** – In this process, material in pellet or filament form is melted and pushed through a nozzle to trace the cross section of each layer. The material solidifies after deposition, gradually building the object.
- **Sheet Lamination (SHL)** – In this method, sheets of material are stacked or bonded to create a part. The production speed is hard to achieve thereby increasing the complexity.

2.3 Process Selection

Among the seven AM technologies discussed in the theory section, those suitable for metal AM and capable of producing components with internal cavities were selected.

Table 2.1: AM Processes – Geometry and Accuracy Comparison (with references).

Criteria	**LMM**	**PBF-LB**	**BJT**	**MJT**
Surface Roughness (Ra)	2–4 µm[23]	10–15 µm[24]	8–12 µm[21]	<2 µm[21]
Dimensional Accuracy	±100 µm[25]	±200 µm[24]	±150 µm[21]	±50 µm[21]
Feature Resolution	50–100 µm[25]	<100 µm[24]	<150 µm[21]	<25 µm[21]

Based on literature, the LMM seemed viable process for copper printing[25]; however, due to the unavailability of furnaces, the process was not investigated further. MJT was also explored, given its better accuracy than BJT, and multi-material printing capability. But due to funding constraints, this technology was dropped. Therefore, out of the four possible processes, two AM processes were considered, PBF-LB and BJT. In the case of PBF-LB, the focus was on the process capabilities and whether the parts can be printed.
Direct Energy Deposition (DED), Sheet Lamination (SHL), and Material Extrusion (MEX) are not feasible for this project due to the various parameters required for a waveguide filter. DED-manufactured parts result in poor mechanical properties [26] and affect layer height, leading to poor geometrical accuracy, as dimensional accuracy is significant for waveguide filters to perform better. The DED part's surface roughness is poor, and post-processing is required to meet the surface finish and tolerances. [27] SHL may not be suitable for complex geometries and not meet the material properties requirements for waveguide filters [28] MEX restricts the ability to achieve intricate fine geometries because the tool head limits layer-by-layer deposition, hindering the precise alignment and deposition required. The surface finish of the MEX-produced part is rough and may require additional post-processing to meet the required surface quality [29].

2.3.1 Binder Jetting Technology (BJT)

This process involves powder deposition and spreading, selective deposition of binder, depowdering, and densification through sintering. The general steps of the BJT process detail the deposition and flattening of a layer of powder onto the build platform. This is followed by the selective deposition of a binder through the printhead. The steps are continually repeated until the part is finished, with each additional layer causing the build platform to descend. The binder bonds with the fine metal powder particles to form "green body" that has the shape of the final component but not the size and the properties. The fragile green body is carefully removed from the powder bed and is sintered to reach the near-full density to provide the required properties to the component. The component will shrink during sintering (upto 20 percent) therefore the component has to be up-scaled to account for shrinkage during the design phase. The part is debinded in the densification process[30]. 2.2 represents the process schematics of BJT.

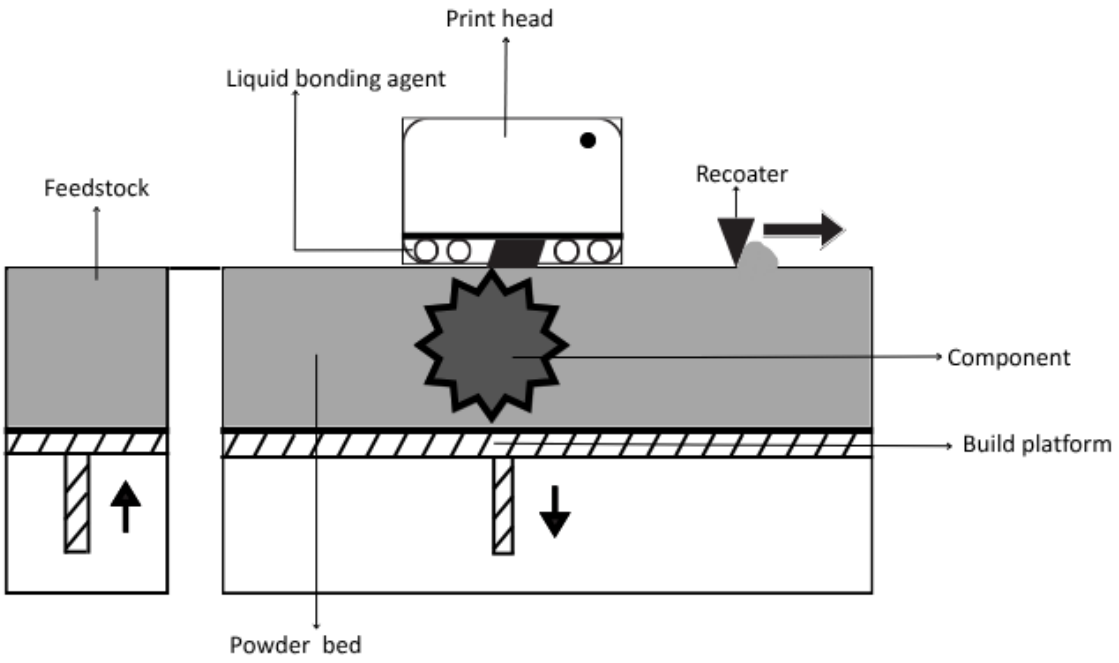

Figure 2.2: BJT Printing process overview.

Advantages include high build rates and low thermal stress due to the absence of high-energy beams in printing. The limitations of BJT include sintering shrinkage, binder residue, and achieving high density in the final part [30]. Single-alloy metals employed for BJT include stainless steels (17-4PH, 304L, 316L), M2 Tool Steel, and alloy 718. The most suitable materials for filters are high electrical conductivity materials like copper. In BJT, complex geometries and intricate shapes can be created with thin walls without requiring support structures. Support structures aren't usually required since the powder in the build chamber acts as support in the printing phase [21]. There is also no involvement of a powerful heat source in BJT, unlike other AM processes, due to the final components do not exhibit

thermally induced stresses and distortions [31]. The orientation of features might impact the roughness of surfaces. For instance, features with varying orientations (0, 22.5, and 45 degrees) relative to the Z-axis exhibited surface quality distinction and density [32]. Components printed using BJT often require costly and time-consuming post-processing to get the final product. Upon completion of the printing process, the components have to undergo debinding and then be sintered to get full densification and the required mechanical properties. Sintering can lead to shrinkages and distortions [21]. A typical BJT surface would have a rough texture compared to conventional processes [33],[31]. The surface roughness Ra values range from 4 µm to 10 µm, varying with process parameters as reported in [32], whereas Sa values range from 3 µm to 13 µm [33].

2.3.2 Powder Bed Fusion Laser Beam (PBF-LB)

PBF-LB is a metal additive manufacturing process in which thin layers of metal powder are spread over a build platform and a high-powered laser selectively fuses these particles according to the geometry of the CAD model [30]. The platform then lowers, a new layer of powder is applied, and the cycle repeats until the whole part is completed. PBF-LB/M uses a high-energy laser source to melt the metal powders completely [1]. A protective inert gas atmosphere prevents oxidation and minimizes contamination. Most of the PBF-LB uses radiative and resistive heaters to heat the powder bed [30]. This layer-by-layer approach facilitates the production of complex geometries with fine details and internal features, offering advantages in weight reduction and design freedom [30]. Weldable metals are suitable materials for use in PBF-LB, such as stainless steel [21]. This technology is capable of manufacturing lightweight complex internal structures. Multiple parts can be printed in a single build.

Surface of PBF-LB is characterized by a coarse texture, requiring post-processing for smoother results [21]. The surface roughness can be impacted by several parameters such as build orientations, process parameters, powder characteristics, among others [12],[34],[35]. The parts oriented at 60 and 90 degrees have the lowest surface roughness. In contrast, the parts oriented above 90 have the highest surface roughness [34],[36]. The surface roughness of PBF-LB components generally ranges from ten to fifty microns [37].

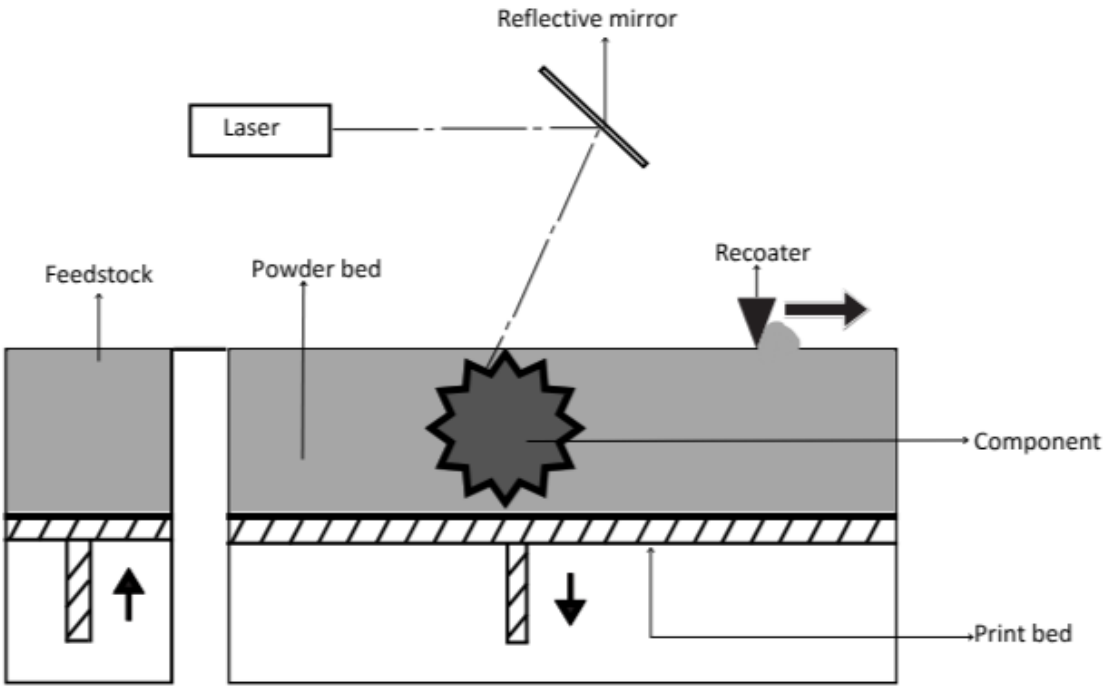

Figure 2.3: PBF-LB process schematics [1].

2.3.3 Lithography based Metal Manufacturing (LMM),

Lithography-based Metal Manufacturing (LMM) is manufacturing by creating a CAD model tailored to the desired geometric and functional specifications [38]. The model is optimized for the LMM process, including part orientation, allowing optimal print quality and production efficiency. In printing, the photoreactive binder in the metal feedstock is selectively cured by a light source, layer by layer, embedding the metal powder and building the desired three-dimensional structure. This produces a green part. The green part undergoes a debinding process conducted thermally or chemically in a special furnace to remove the polymer binder and form a porous brown part made only of metal powder. The brown part is high-temperature sintered, a process in which the metal particles fuse to form a dense, solid body with the desired mechanical properties [38]. The surface roughness of LMM components would range between 2 µm to 4 µm in the as-sintered state [23].

2.3.4 Material Jetting Technology (MJT)

Material Jetting (MJT) is another advwanced AM technique, defined by the deposition of build and support materials in the form of controlled droplets onto a build platform. These droplets, dispensed via nozzles, are subsequently solidified, often using UV light in the case of polymers. MJT includes both continuous and discontinuous (drop-on-demand) jetting methods. While polymer jetting is well established, metal jetting is an emerging field involving molten metal droplets. The technique is known for its precision and ability to build complex structures with

smooth surface finishes, high speed, and multiple materials [39]. The capability of MJT to incorporate multi-material printing within a single build volume represents a promising direction for future device fabrication rather than mere part production [39].

2.4 Design for AM (DfAM)

When designing a product that is to be manufactured using additive manufacturing, a concept known as Design for AM comes into play, which can enable designers to think outside the box of the traditional manufacturing perspective [40]. AM has benefits from materials, unique geometry to customization. AM has the potential to fabricate virtually any shape, and it can fabricate fully operational assemblies in a single build [21]. DfAM can enable designers to think of designing products by focusing on AM-specific challenges such as overhangs, stair-stepping effect, anisotropy, and the need for reduction of support structures [40]. Given AM's design freedom, ability to fabricate complex geometries, it can enable monolithic design [12]. This can be valuable to Ericsson in designing RF components incorporating different functionalities such as electromagnetic, mechanical, and thermal.

2.5 Post-treatment - Electroless Copper Plating (ECP)

The electroless copper plating method is based on a chemical reaction between a reducing agent and a copper salt in an aqueous solution [2]. This reaction reduces copper ions to copper atoms. This reaction should be continuous for the resulting copper film to be thick enough to adequately cover the substrate. This process is extensively utilized in the printed circuit board manufacturing industry to transform non-conductive substrates into conductive material for subsequent electroplating and to enable the plating of holes [2].

Electroless copper plating uses a solution that is primarily composed of cupric sulfate as the copper ion source and EDTA as a complexing agent, where glyoxylic acid is used as the reducing agent. Plating is carried out at 45°C or 60°C based on composition, with aeration to both optimize stability and minimize decomposition [2].

Surface preparation consists of degreasing in 5% NaOH, followed by micro-etching 5% to promote adhesion. Neutralization with NaOH precedes substrate conditioning with a 5% HCl soak and catalyzing with a palladium-tin colloidal solution. Catalytic particles required for plating reaction initiation are left behind and is rinsed with deionized water between operations to remove residual chemicals [2].

The catalyzed substrate is submerged in the hot plating bath. After the depositing process, a soak in 5% sulfuric acid is done to leave an anti-tarnish protection, which then follows rinsing and drying [2].

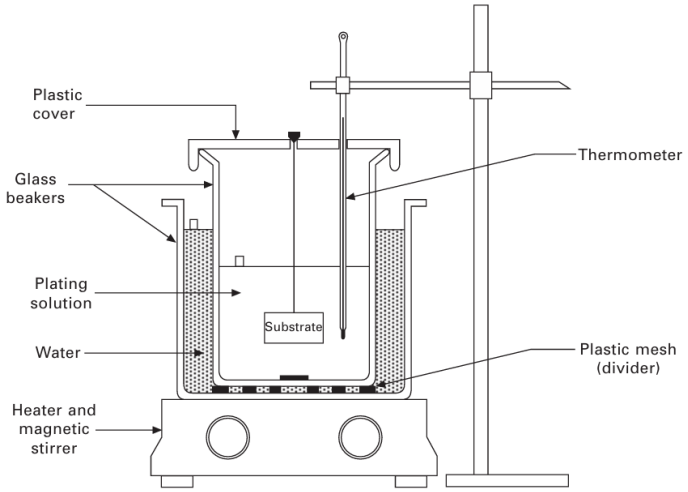

Figure 2.4: Apparatus for Electroless Plating [2].

2.6 Surface roughness

Surface roughness, in general, portrays the presence of geometrical irregularities on the surface. It is a component of a much broader concept of surface texture, which entails the repetitive and random deviations from nominal surface topography. Surface roughness can be characterized by different parameters, such as amplitude parameters like Ra/Sa(arithmetic average) and Rq/Sq(root mean square), which quantify the height variations.

$$Ra = \frac{1}{L}\int_0^L |z(x)|\,dx, \qquad Sa = \frac{1}{A}\iint_A |z(x,y)|\,dx\,dy$$
$$Rq = \sqrt{\frac{1}{L}\int_0^L z^2(x)\,dx}, \qquad Sq = \sqrt{\frac{1}{A}\iint_A z^2(x,y)\,dx\,dy}$$

Other amplitude parameters include skewness(Ssk/Rsk), kurtosis(Sku/Rku), and peak-to-valley height(Sz/Rz).

$$Rsk = \frac{1}{Rq^3}\cdot\frac{1}{L}\int_0^L z^3(x)\,dx, \qquad Ssk = \frac{1}{Sq^3}\cdot\frac{1}{A}\iint_A z^3(x,y)\,dx\,dy$$
$$Rku = \frac{1}{Rq^4}\cdot\frac{1}{L}\int_0^L z^4(x)\,dx, \qquad Sku = \frac{1}{Sq^4}\cdot\frac{1}{A}\iint_A z^4(x,y)\,dx\,dy$$

$$Rz = \frac{1}{5}\sum_{i=1}^{5}(z_{p,i} - z_{v,i}), \qquad Sz = z_{\max} - z_{\min}$$

$$Rsm = \frac{1}{n}\sum_{i=1}^{n} S_i$$

Surface roughness can be measured in two different methods, profile(2D) and areal(3D) methods. In the profile surface roughness method, the surface is characterized along a single line or a profile. Whereas areal(3D) surface roughness provides a 3D description of the surface. The arithmetic mean deviation (Ra) gives a baseline view of surface roughness. Rsm provides a measure of the average spacing of surface features. Rz is the peak-to-valley height useful in accessing the average height between the highest peaks and the lowest valley in a surface profile. In the case of Sa, the average areal height is similar to that of Ra but is measured over a surface patch. Sq, root mean square height gives a comprehensive, three-dimensional characteristic of the AM surface. Sz peak-to-valley roughness is analogous to that of Rz but measured over an area [41].

2.6.1 Surface Roughness in AM

AM surfaces, compared to conventional manufactured surfaces, have higher surface roughness [42]. The average surface roughness (Ra) of 5-25µm is exhibited from the PBF-LB and BJT surfaces. Depending on the print orientation and the presence of adhering powder particles, PBF-LB surfaces have a high surface roughness of Sa 5-25µm [36]. AM surface is characterized by irregularity in the surface, and sharp protrusions. Some other contributing factors to the appearance and roughness include adhering powder particles, spatter formation, loose or partially melted particles, and fill patterns [41]. AM being a layered manufacturing process, a common issue of stair-step arises on slanted or curved surfaces [41]. In case of BJT, sinter can reduce the roughness; however, the texture remains more than conventionally manufactured surfaces [33]. In Powder Bed Fusion (PBF) processes, downskin surfaces often have a significant amount of partially melted or non-melted powder particles attached, while upskin surfaces are typically free of powder [35]. Downskin surfaces tend to be composed of mostly valleys, or a combination of peaks and valleys, whereas upskin surfaces are predominantly peaks [35].

2.6.2 Surface Roughness Measuring Techniques

International Standards provide well-established regulations to ensure consistency in surface roughness assessment. The ISO 4287 standardizes the system of 2D roughness parameters, and the ISO 25178 [43] [44] standardizes 3D areal texture analysis. Most recently, ISO 21920 [45] [46] [47] updated the notation of surface finish specifications for application in technical documentation, which has improved clarity in design and manufacturing. Surface roughness can be measured by contact and non-contact methods, both of which have their advantages. Non-contact techniques like optical interferometry and laser scanning confocal microscopy provide high-resolution 3D surface imaging without touching the surface. These techniques are advantageous for microscale features as they do not carry the risk of surface deformation [48]. However, one of the limitations of using an optical microscope is that shading effects affect data capture of the curved surfaces [42]. In this thesis project, a laser confocal microscope is used for measuring both profile and areal surface roughness. According to ISO standards, selecting a cutoff length of 2.5 mm

is ideal for measuring the profile surface roughness [49].

3

Methods

The RF waveguide filter was designed by Klas Eriksson at Ericsson AB. The design had been made not from an AM perspective but from a milling point of view as a result the filter contains sharp edges and turns. Initially, a 90-degree bend was added to the internal channel at each end.

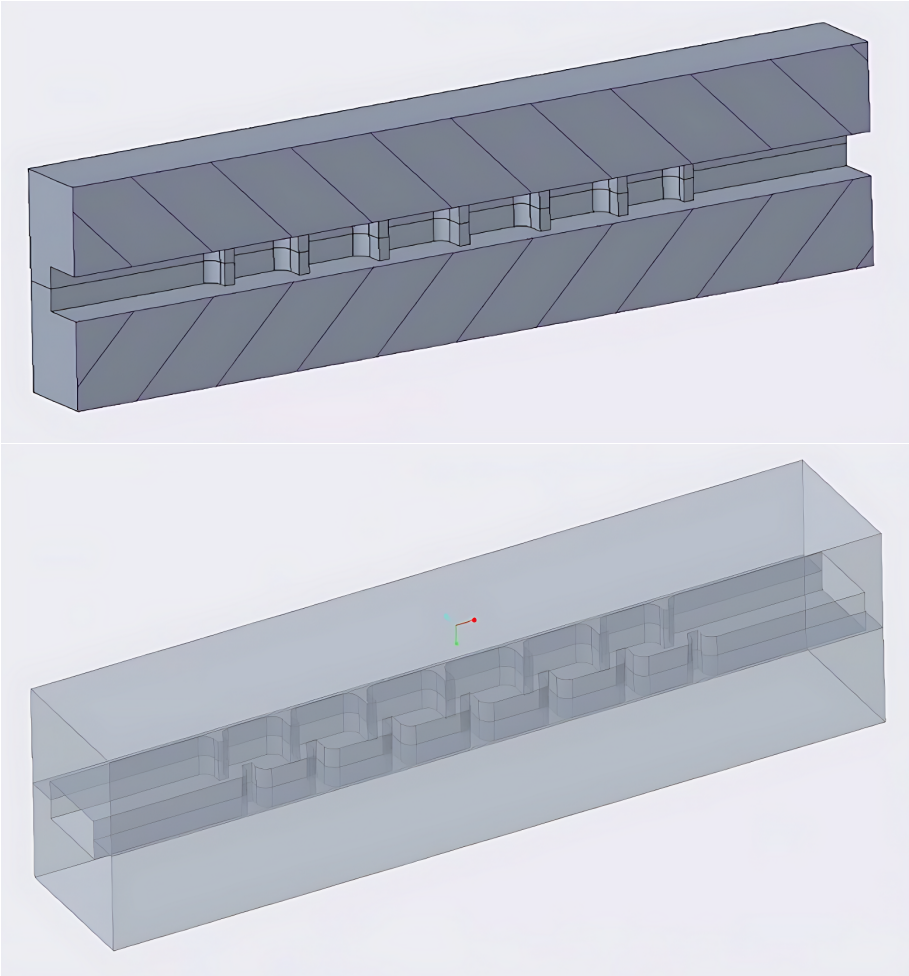

Figure 3.1: Waveguide filter design.

Stainless steel 316L was used to manufacture the components for printing in both technologies BJT and PBF-LB due to the unavailability of copper.

3.1 Iteration of printing and evaluation

The waveguide filters are designed for D-Band and E-band frequencies. Specific D-Band frequency range for the filter is 65 GHz to 67 GHz, for E-Band, it is 130 GHz to 134 GHz.

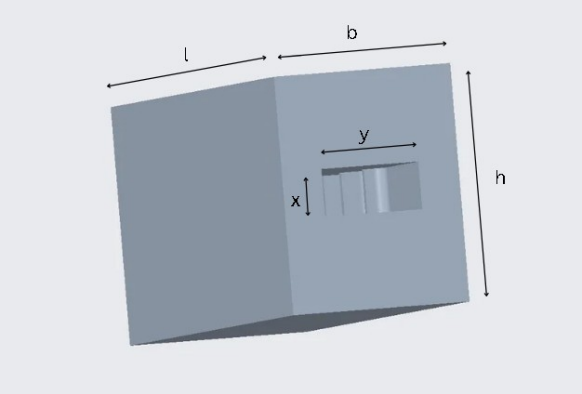

Figure 3.2: Filter Dimensions.

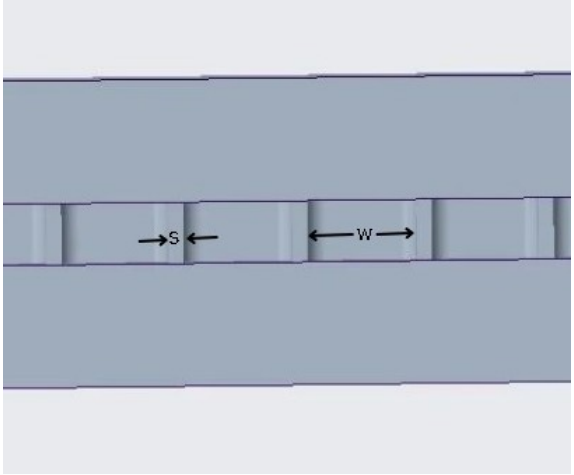

Figure 3.3: Filter fins and cavity Dimensions.

Table 3.1: Dimensions of Filters in mm

Filter	l	b	h	x	y	s	w
E	32	6	8	1.6	3.2	0.40	2.840
D	16	3	4	0.8	1.6	0.20	1.410

3.1.1 Printing with PBF-LB process

The powder particle size distribution in PBF-LB is 20 µm to 65 µm. Parts printed using PBF-LB were produced at Chalmers with an EOS M100 machine. Part orientation and build preparation were performed in Materialize Magics software. Each part was indexed for better traceability. For instance, E1BSLM refers to an E-Band

filter built at plate position 1 by SLM (PBF-LB). Parts oriented between 60-75 degrees yielded better surface roughness than parts oriented in 30 - 45 degrees, and >90 degrees [34]. The parts were oriented at a 60-degree angle. Orienting the part below a 60-degree angle led to the formation of support structures within the internal fins, which would have been very difficult to remove as the fins are the most essential parts of the component. All these simulations were conducted in the build preparation software of EOS M100 machine as shown in the figure 3.1.

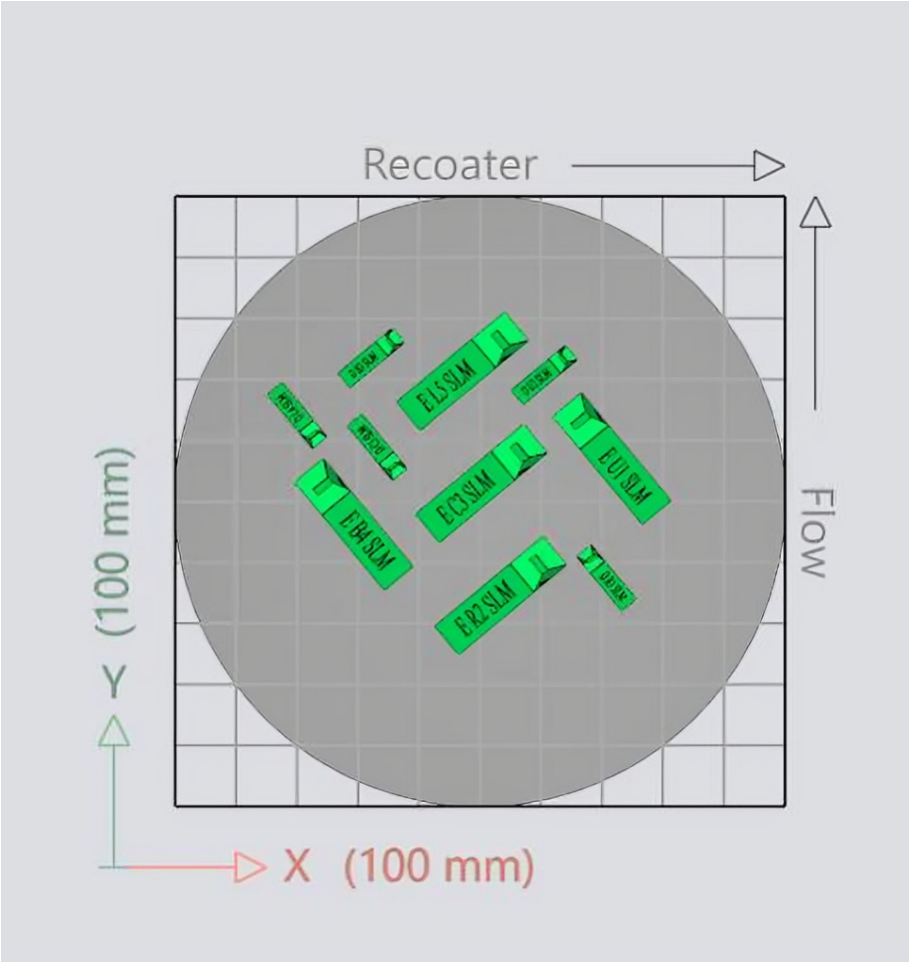

Figure 3.4: PBF-LB Orientation in Materialise Magics.

The design parameters considered were :

- Support structure height: 2 - 3 mm of support height was added to ensure sufficient height for the cutting operation.
- Machining: The completed parts were cut from the build plate with a band saw, and support structures were milled.

The processing parameters were as follows:

- Layer thickness: 20 µm
- For machine parameters, the scan speed and gas flow, standard EOS parameters were followed.

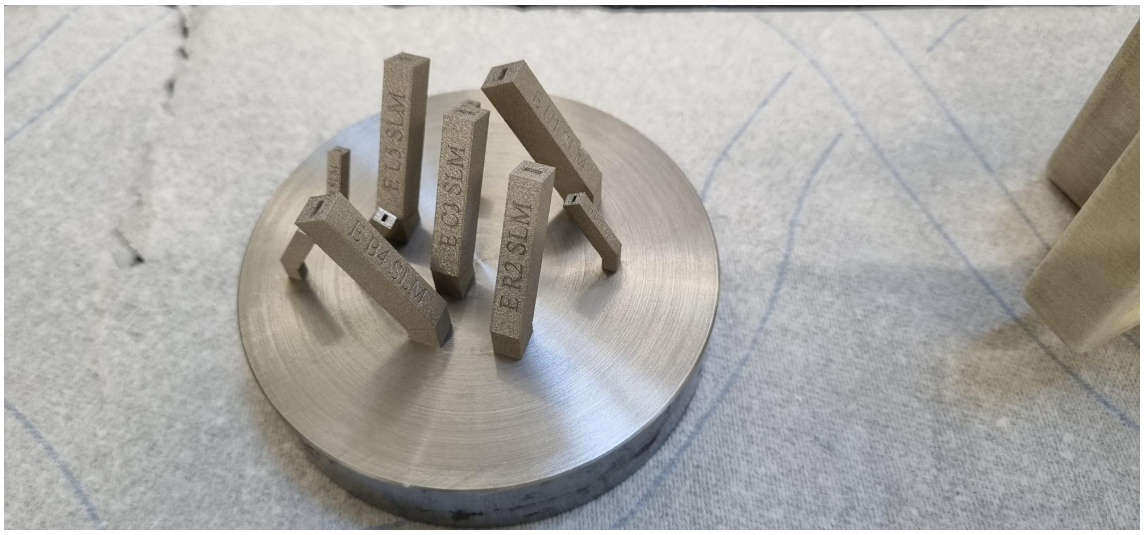

Figure 3.5: PBF-LB Printed parts with supports.

The manufacturing was conducted at CTH under the supervision of the Academic supervisor Erika Tuneskog.

3.1.2 Printing with BJT process

A total of 40 components were manufactured by Bosch GmbH with BJT. The manufacturing took place in two phases. The first was a trial run where the objective was to evaluate process capability and also perform surface roughness measurements. Components were printed in three different orientations X, Y and Z straight in the axis direction as shown in 3.6. The parts oriented at an angle to the axis direction results in a worse surface finish, as shown in 3.7. Different surfaces were evaluated, the outer surface with engraving, one opposite to the engraved side, and two more in assumed internal surfaces, as shown in 3.8. It is unclear which surface in the internal channel has more influence on the functionality of the components. Due to this, Bosch assumed one cross-section of the part and measured the surface roughness. In the X-oriented part, all four measurements were conducted. However, in parts oriented Y and Z, the product critical area (internal structures with fins) was chosen for the surface roughness measurement. Considering the product critical area measurements for all orientations X, Y, and Z, it was observed that Y-oriented parts gave better surface roughness measurements as shown in 3.2.
The results from the first trial of measurements for surface roughness are as follows in the table 3.2.
It was also observed that there were leftover powder particles in the channel which were not been able to be removed after depowdering. To view this, the components were sanded down as shown in 3.9 . Additionally, more effort had to be given during the depowdering procedure for the next print job to ensure sufficient powder removal within the channel.

Upon completion of this trial run, the final printing job was performed. A total of 40 components were printed. 20 of which were E Band waveguide filters, and the

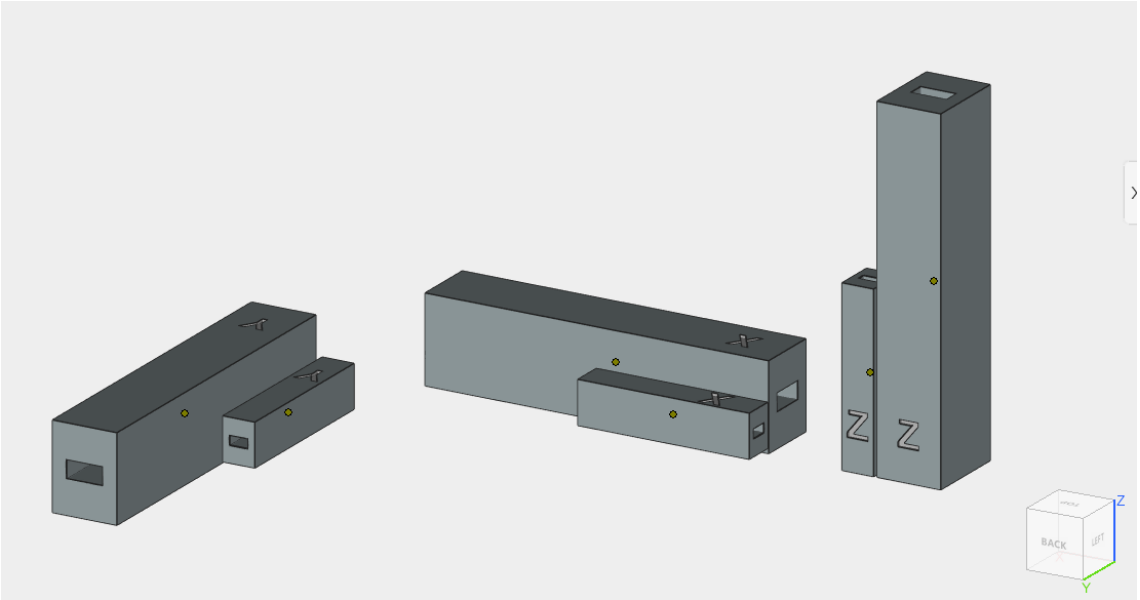

Figure 3.6: Orientations for BJT.

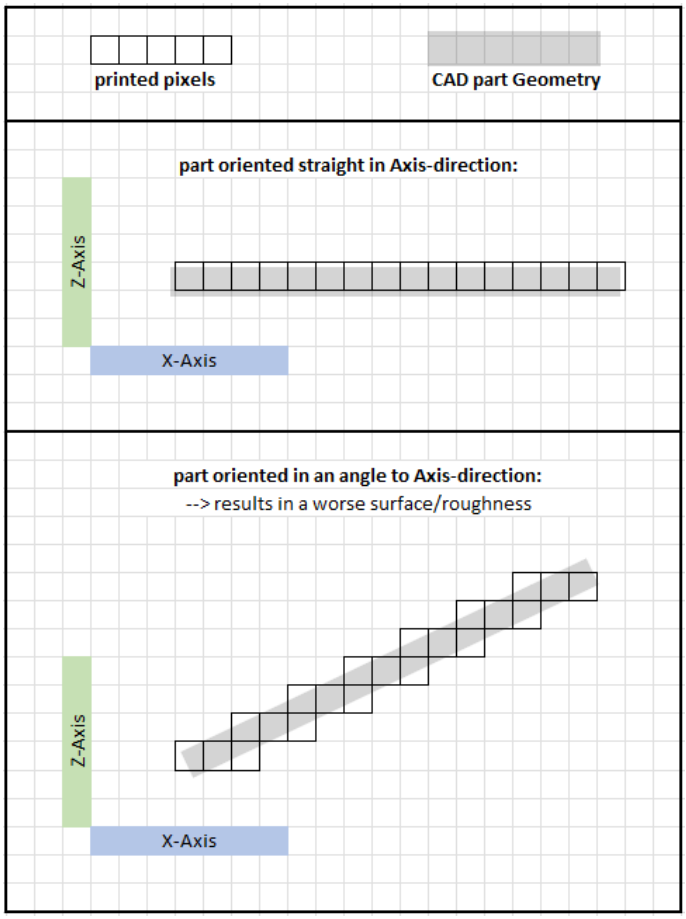

Figure 3.7: Axis direction of BJT components.

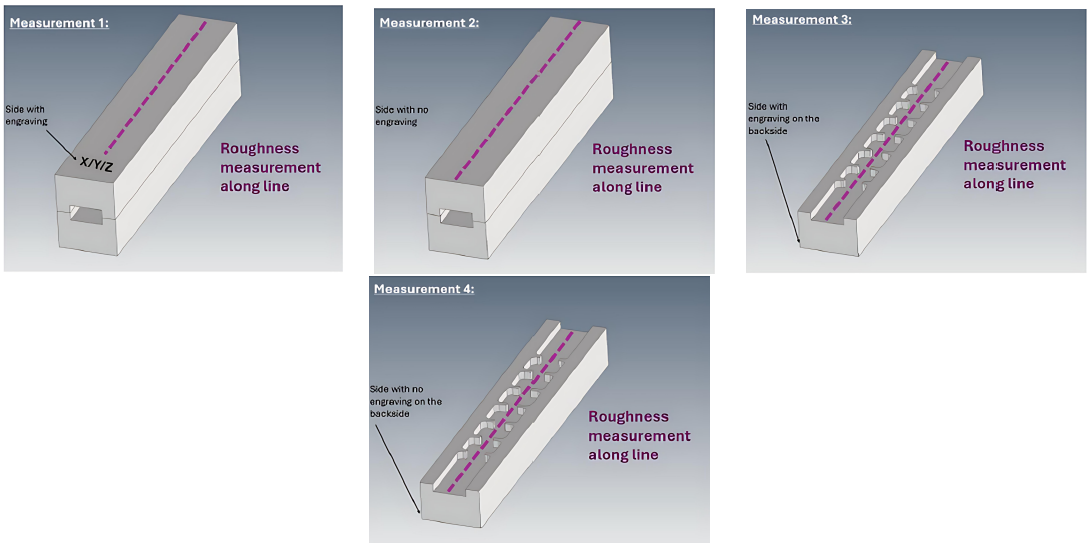

Figure 3.8: Roughness measurement of BJT components from different sides.

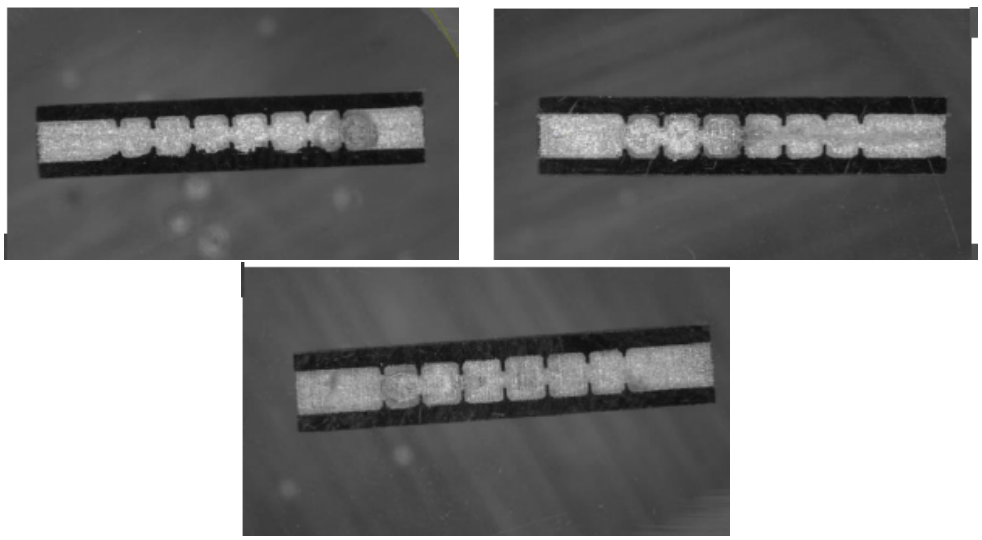

Figure 3.9: Intersected parts of BJT components from different sides.

Table 3.2: Results from the surface roughness measurement after the trial (Dimensions in μm)

Part Orientation	Plane Measured	Ra (Avg.)	Rz (Avg.)	Rp (Avg.)	Rv (Avg.)	Rc (Avg.)	Meas. Length (μm)
X	Measurement 1	3.3	28.4	13.8	14.6	19.0	9495.9
X	Measurement 2	6.4	52.8	26.6	26.2	33.4	14504.8
X	Measurement 3	5.8	44.4	22.0	22.4	31.7	14504.8
X	Measurement 4	4.9	47.5	17.7	29.8	27.3	14504.8
Y	Measurement 4	3.6	42.6	20.8	21.7	24.5	14504.8
Z	Measurement 4	9.2	81.1	44.2	37.0	49.6	14504.8

rest 20 were D Band waveguide filters. All parts were indexed from E1 to E20 and D1 to D20 for E-Band and D-Band filters, respectively.

3.2 Surface treatments

Because of the low conductivity of the stainless steel 316L surface treatment of the high frequency filters was required for the electrical specification. Electroless copper plating was chosen for plating the filters. The initial electrical tests before the plating resulted in poor performance by PBF-LB-produced components, whereas BJT-produced components gave the best results. Therfore, 5 E-Band filters E8, E14, E12, E2, E15, and 5 D-Band D2, D3, D5, D6, D7 filters produced by BJT were chosen for plating, which is based on their electrical test performance, in other words, for their low insertion loss and good resonance center frequency. The plating was done by Provexa AB.

3.3 Electrical characterization

Electrical measurements were conducted on a total of 46 printed components. The final sample set included:

- 6 filters printed using PBF-LB
- 40 filters printed using BJT

Electrical measurements were performed at Ericsson's RF lab using Vector Network Analyzers (VNAs) under the supervision of Klas Eriksson. The scattering (S11, S21, S12 and S22) parameters were measured over the frequency ranges of interest of the D-Band (130-135 GHz) and E-Band (65-67 GHz) filters. These measurements were used as the reference standard for assessment of design accuracy, internal surface quality, and overall functionality of the component. Upon completion, the traces collected from the electrical characterization and plotted together in MATLAB. Comparative graphs were plotted to showcase the electrical performance of BJT and PBF-LB parts, along with simulated electrical performances as well.

Figure 3.10: E Band Electrical test setup.

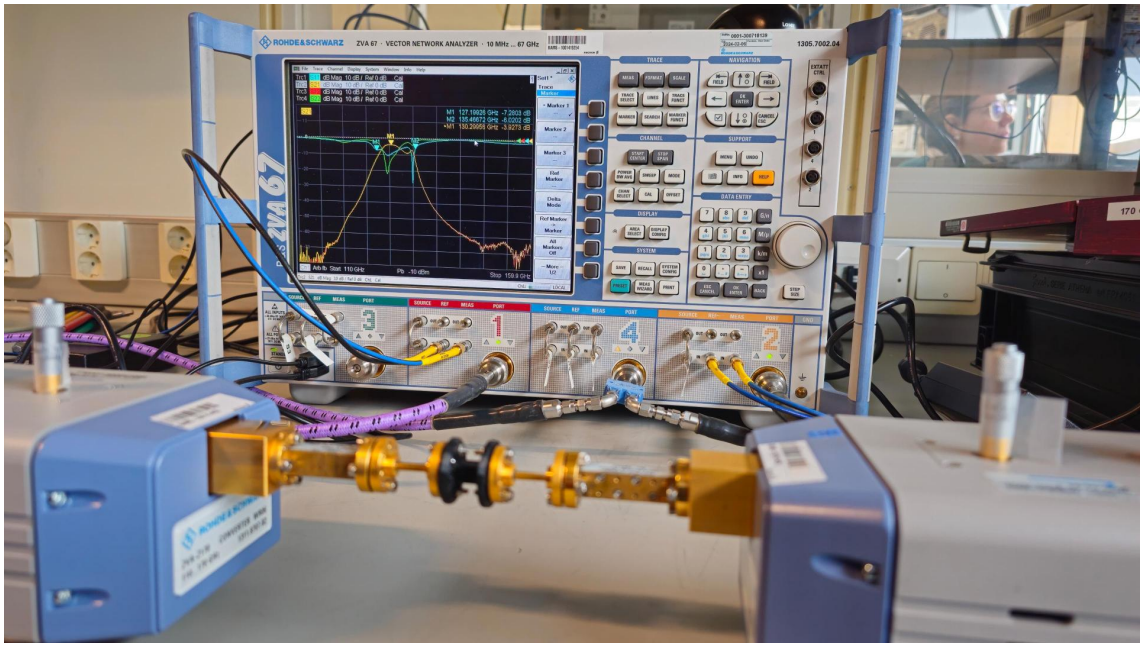

Figure 3.11: D Band Electrical test setup.

For electrical testing purposes, separate fixtures for each band were designed using PTC Creo and printed at the Ericsson facility as shown in figure. These fixtures were used to hold the filters between the waveguide flanges for the electrical testing. Two different types of 3D printers were used to print these fixtures: an FDM printer and a VPP printer. Fixtures printed using the FDM printer (Stratasys F370) had poor surface finish and dimensional accuracy. However, fixtures printed using a VPP printer (FormLab Form 3) had a smoother finish and higher dimensional accuracy.

The fixtures produced from both printers were used for electrical testing.

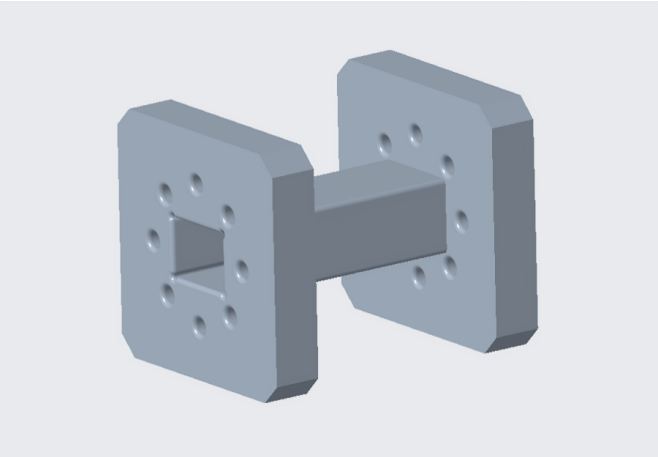

Figure 3.12: Fixture for E-Band filter.

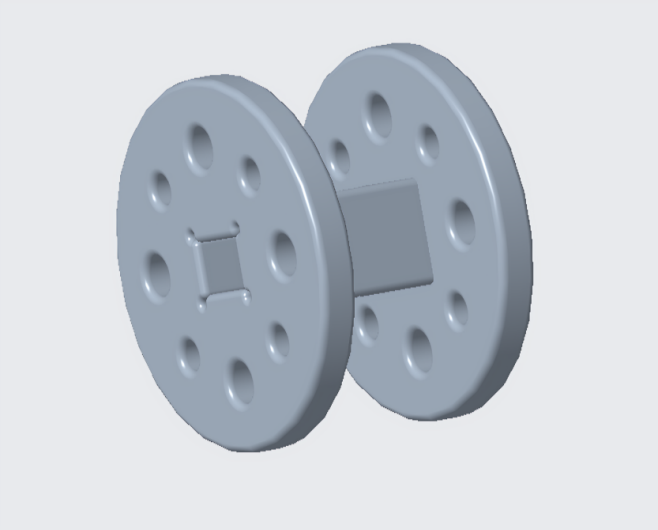

Figure 3.13: Fixture for D-Band filter.

3.4 Dimensional and surface characterization

The functionality of the filters relied more on the internal channels; therefore, the focus was on the internal features for both dimensional and surface characterization. The outer surfaces were measured using a digital vernier caliper with an accuracy of ± 0.02 on multiple sides of the same component, and the average of those measurements was considered. The components were split into two different cross-sections as shown in the , using a milling machine and a diamond saw cutter. An optical microscope, Keyence VHX X1 in 3.16 was used to measure the internal dimensions. The fins and cavity within the internal channel were measured for the filters made by both BJT and PBF-LB.

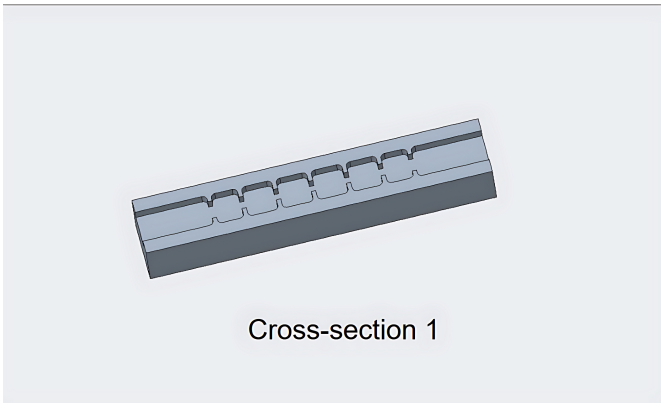

Figure 3.14: Cross-section of the component 1.

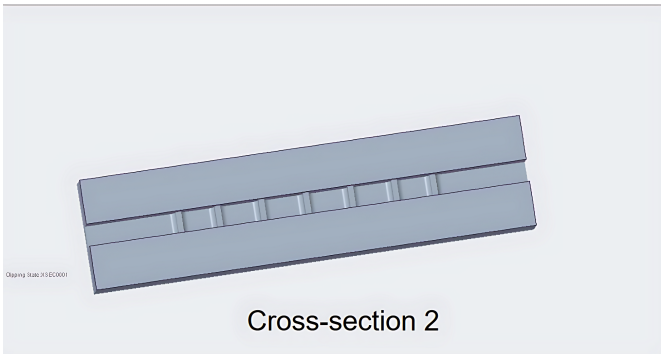

Figure 3.15: Cross-section of the component 2.

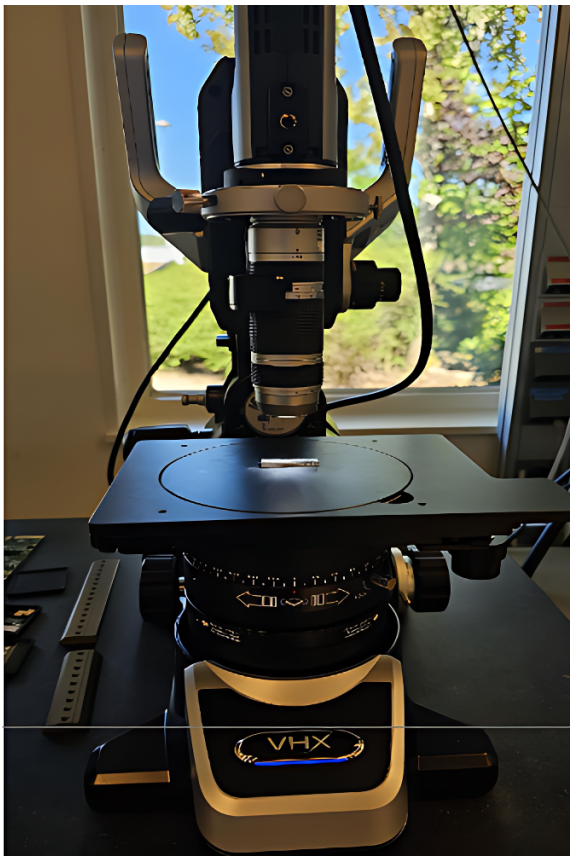

Figure 3.16: Keyence VHX X1 Optical Microscope.

The types of roughness considered were profile roughness and areal roughness. A 3D laser confocal microscope, the Keyence VK-3000 laser microscope in 3.17 was used at the Ericsson Borås facility to measure the surface roughness. Magnifications of 2.5X and 5X were used to measure both types of surface roughness. The noise from the captured scan was removed in the machine settings. The cut-off length for E-Band filters was set to 2.5mm, adhering to the standards, assuming a rough surface of the AM surface, a sampling length of 2.5 mm [50] was considered to obtain a reliable result.

Figure 3.17: Keyence VK-3000 Laser Microscope.

Furthermore, Ra, Rz, and Rsm were considered for profile surface roughness. Higher magnification meant smaller sampling length; due to this, standard measurement processes could not be adhered to in all the surface roughness measurements. Therefore, for the D-band standard sampling length could not be met. For measuring the areal surface roughness, similar machine settings were used. It was measured in two ways, one in which the surface of one cavity was evaluated, and in the other, a straight surface within the internal channel was used, as highlighted in 3.18 . Similar to the profile method, Sa, Sq, and Sz surface roughness were measured. A laser microscope was an option to map the whole outer profile, however, it would require a stitching procedure to map the whole region, which wasn't available due to licensing issues.

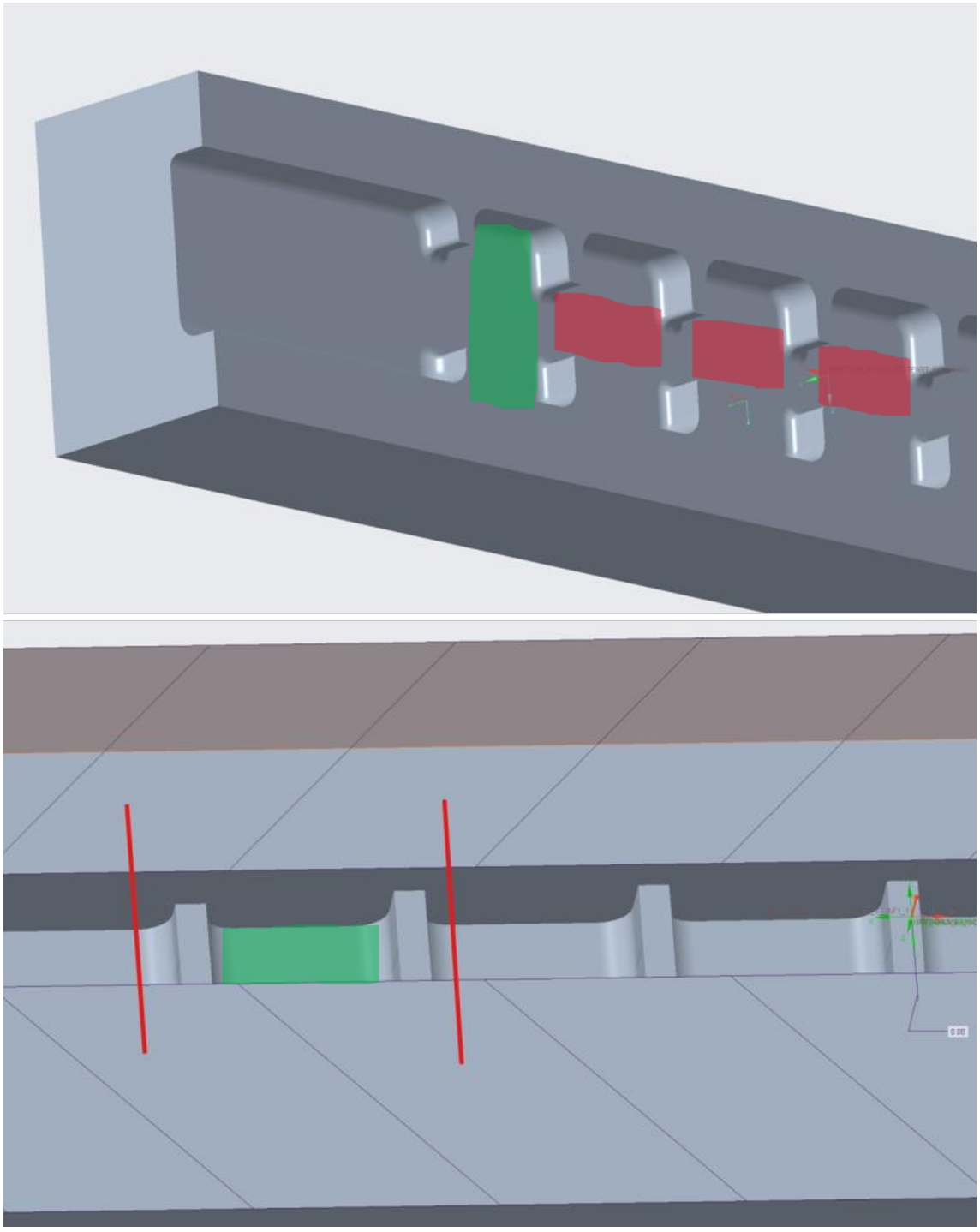

Figure 3.18: Surface roughness measurement Profiles.

3.5 Printing Defects

The ECP was difficult to perform for the design as intimated by the surface treatment vendor, Provexa AB. Printing defects occurred in both PBF-LB and BJT processes. In PBF-LB, the defect occurred on the outer edge of the filter as shown in 3.21. In the case of BJT, the defect was within the internal cavity of the filter,

which was detected as shown in 3.20after electrical testing, due to the extremely high insertion loss(S21) of -21.69 dB as shown in 3.19.

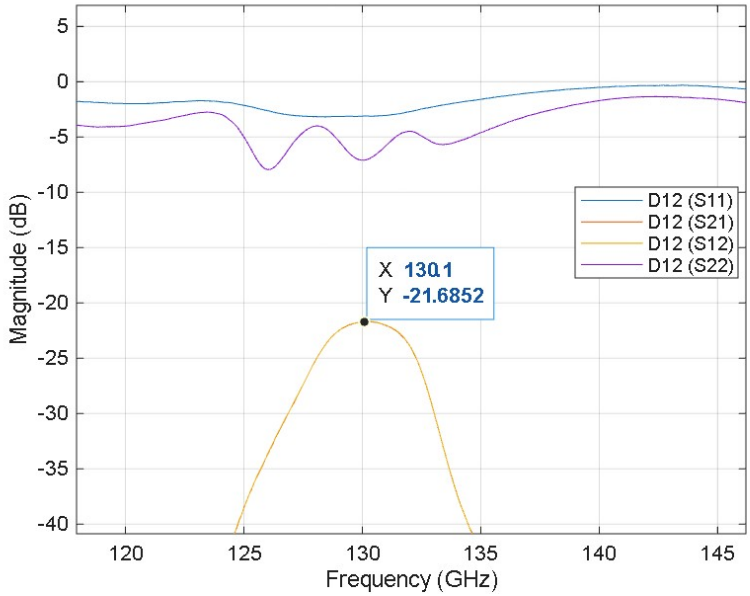

Figure 3.19: Frequency vs loss magnitude plot for D12 filter.

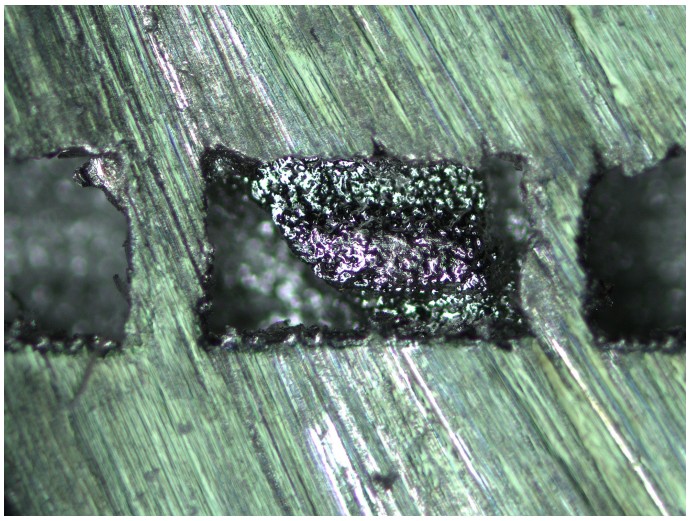

Figure 3.20: BJT Filter D12 printing defect.

Figure 3.21: PBF-LB filter EU1 SLM.

4

Results

4.1 Electrical Characterization

Four S-parameters (S11, S21, S12, and S22) were obtained for each of the 40 BJT components and 6 PBF-LB components using the VNA. Upon extracting the traces, they were plotted using MATLAB. According to Ericsson's product specifications of a filter, a good filter has the magnitudes |S11| and |S22| <-15dB and |S12| >-0.6dB (E-Band) >-1.0 dB (D-Band) in the passband. Since the material used in the project is SS316L, it is was expected that the filter would have high losses. A simulation was carried out for SS316L D-Band filter in ANSYS HFSS, which provided a nominal peak loss of -3.64 dB and peak frequency of 132.1 GHz4.1.

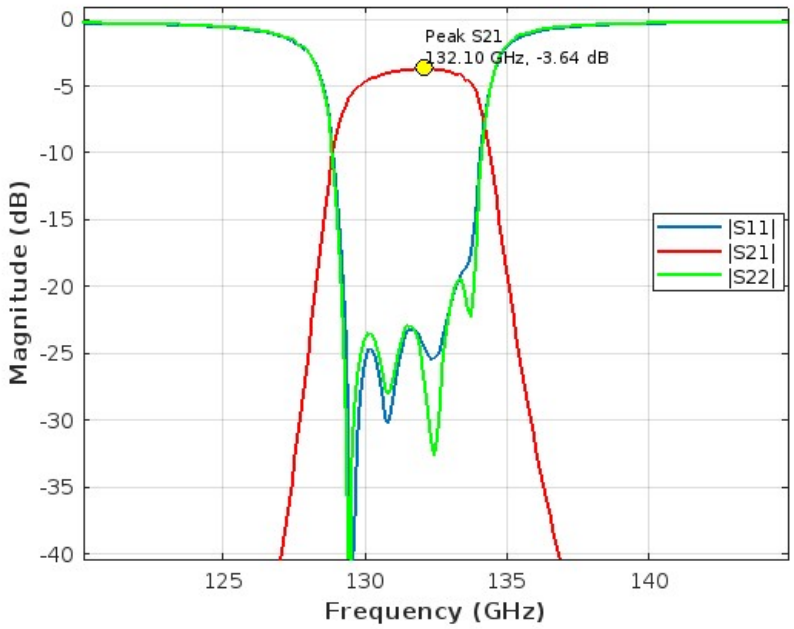

Figure 4.1: Frequency vs magnitude plot for simulated D-Band filter.

In 4.2, 4.3, the output of select E-Band filters E14 and E15, which have insertion losses near -3dB, an acceptable range for an SS316L filter. In 4.4, 4.5, the output of select D-Band filters D3 and D6, which had insertion loss close to -5 dB. Given the material being SS316L, it is expected to to have this loss magnitude.

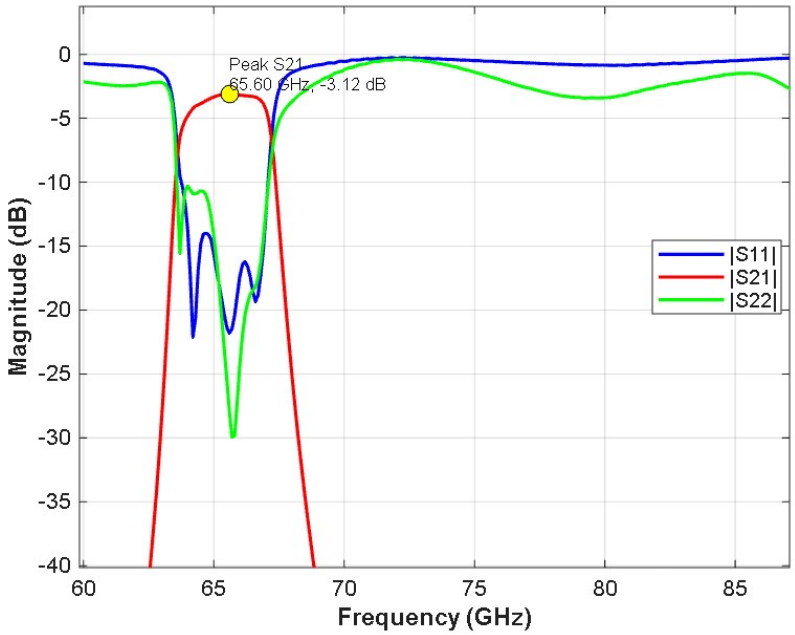

Figure 4.2: Frequency vs magnitude plot for E-Band filter, E14.

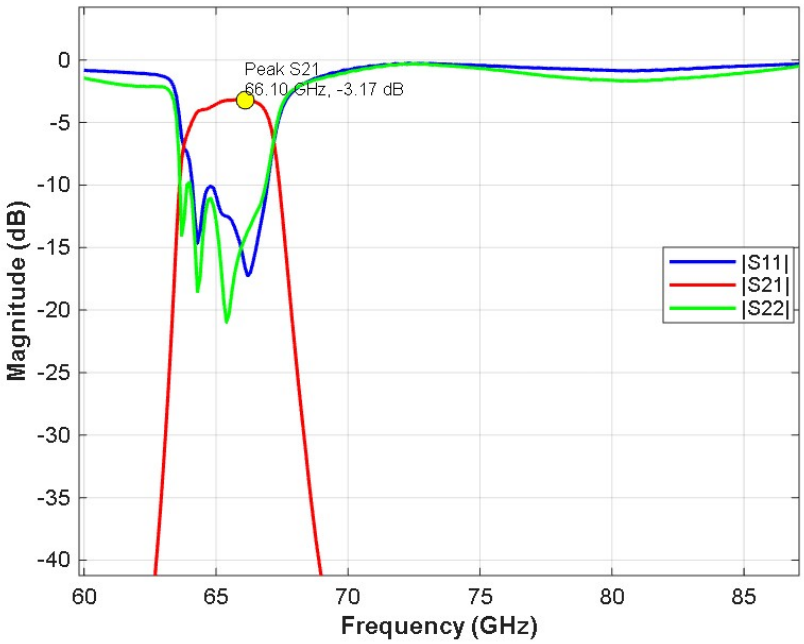

Figure 4.3: Frequency vs magnitude plot for E-Band filter, E15.

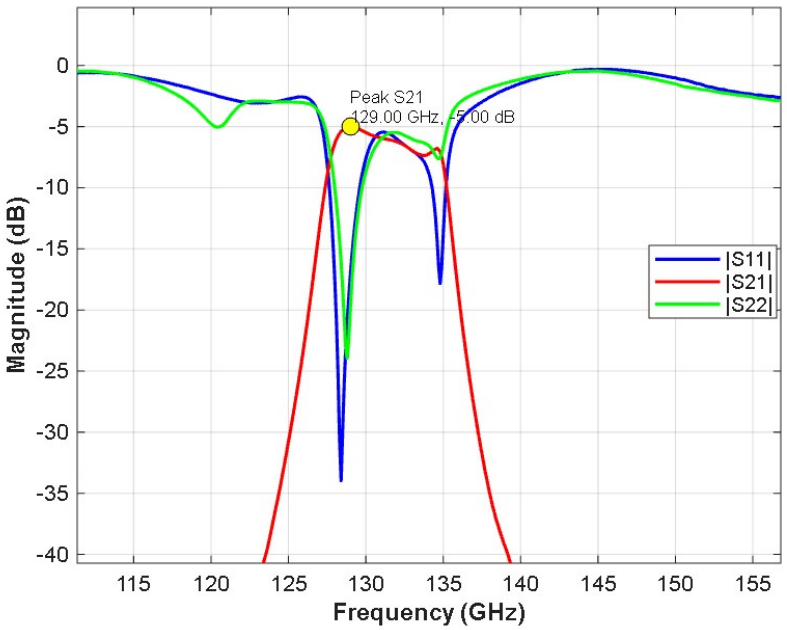

Figure 4.4: Frequency vs magnitude plot for D-Band filter, D3.

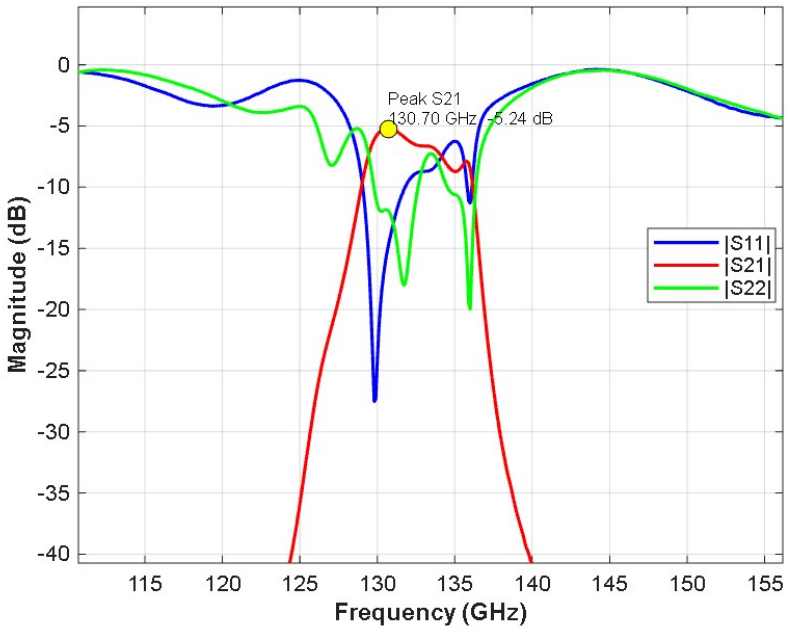

Figure 4.5: Frequency vs magnitude plot for D-Band filter, D6.

In the case of PBF-LB, similarly, the plots were created for all 10 components, 5 for each D-Band and E-Band. To distinctly specify the S21 and S11 curves, separate plots were created. Three of each bands were selected. For E-Band filters 'E L5 SLM', 'E R2 SLM', and 'E U1 SLM' were selected 4.6, 4.7. For D-Band filters 'D R1 SLM', 'D C5 SLM', and 'D B2 SLM' were selected 4.8, 4.9. The losses came out

to be too high for the filter to be functionally useful.

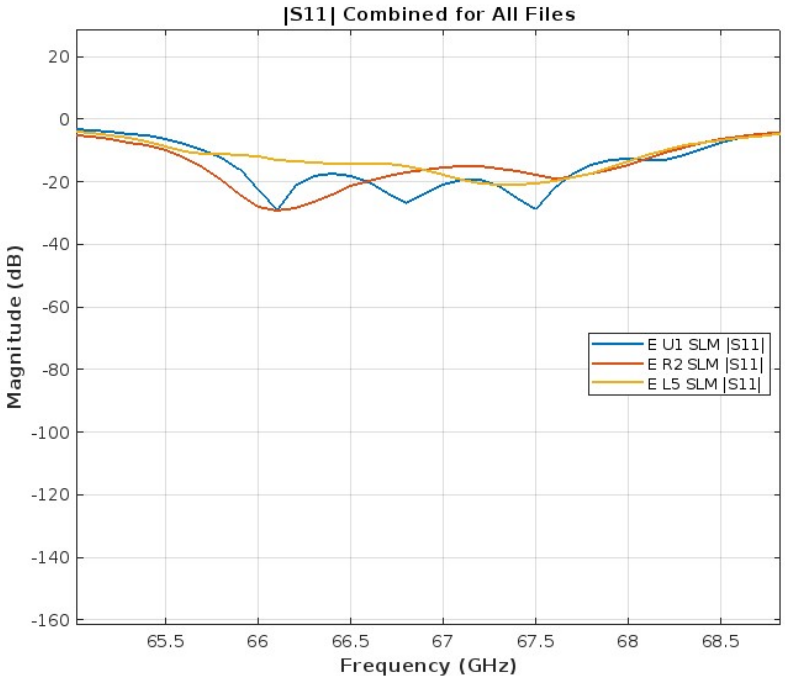

Figure 4.6: PBF-LB, E-Band frequency vs magnitude plot — S11 parameter.

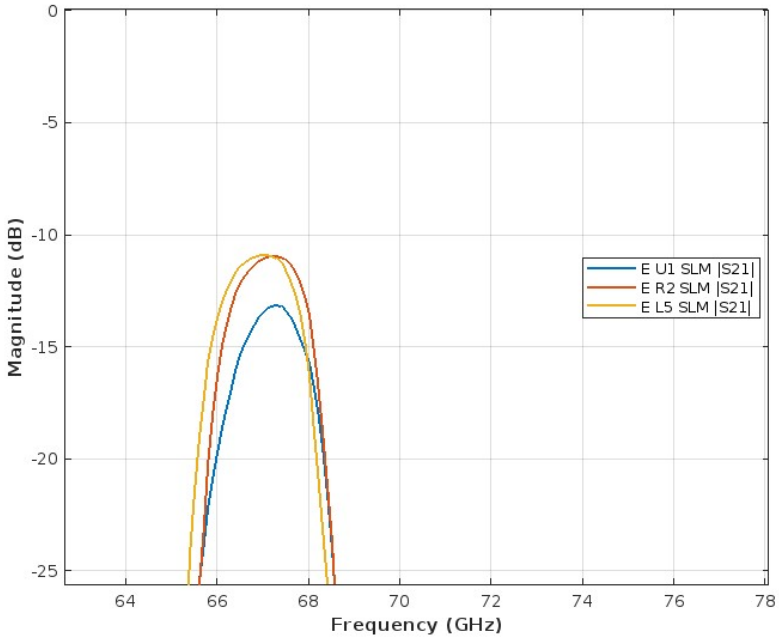

Figure 4.7: PBF-LB, E-Band frequency vs magnitude plot — S21 parameter.

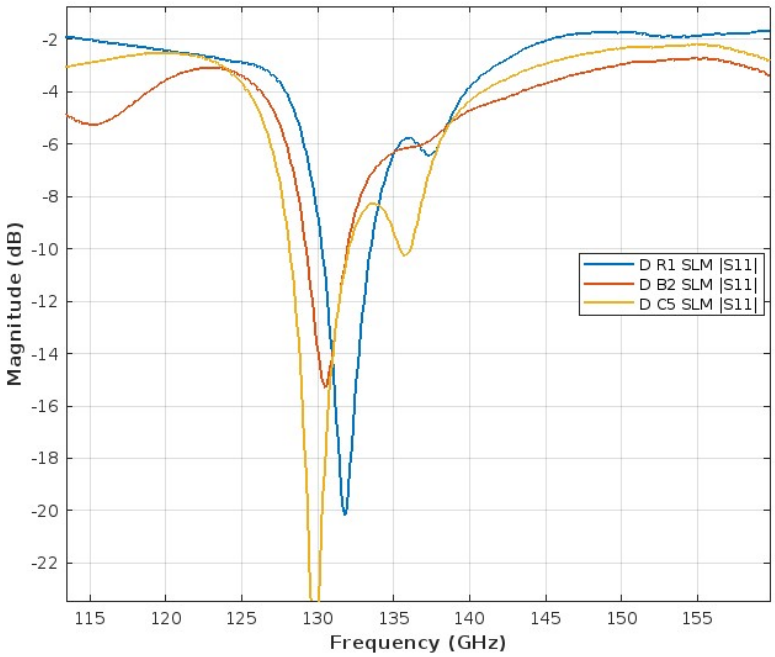

Figure 4.8: PBF-LB, D-Band frequency vs magnitude plot — S11 parameter.

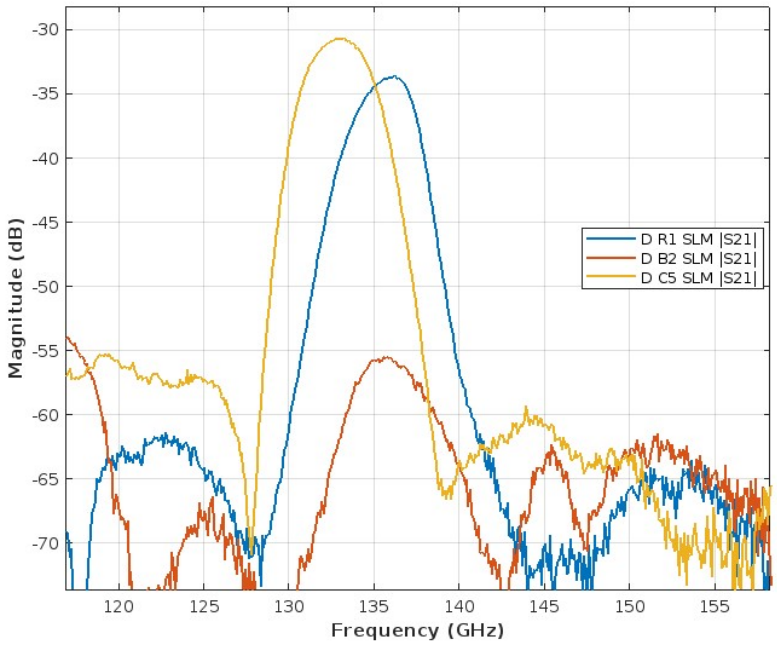

Figure 4.9: PBF-LB, D-Band frequency vs magnitude plot — S21 parameter.

Multiple traces were recorded for each filter to better characterize measurement errors, particularly in D-Band filters during testing. The spread in frequency and responses is related to the measurement error. The flatness in the S21 curve would

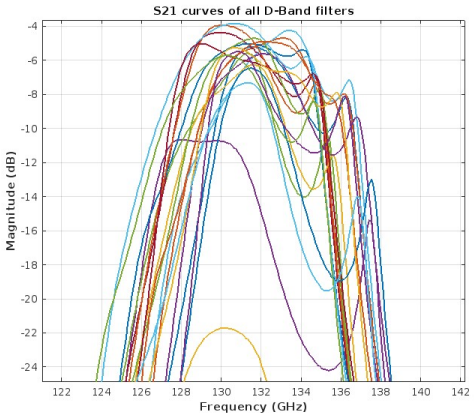

Figure 4.10: S21 curve of all D-Band filters.

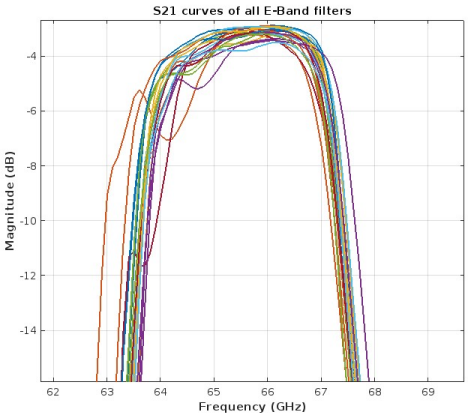

Figure 4.11: S21 curve of all E-Band filters.

relate to the required frequency band being transmitted within the filter. In case of E-Band filters as in 4.11, the S21 curve is relatively flat with a couple of filters having slight deviations. However, in D-Band filters as illustrated in 4.10, there is no flatness in the S21 curve except for a select few, as highlighted in 4.4 and 4.5. This occurrence can be equated to the error. Furthermore, to verify this error, the D-Band filters were further investigated by taking multiple VNA plots of single filters. For this purpose, electrical characterization was performed five times for each of the BJT filters D8 and D16, to demonstrate the shift in loss magnitude for each test 4.12, 4.13.

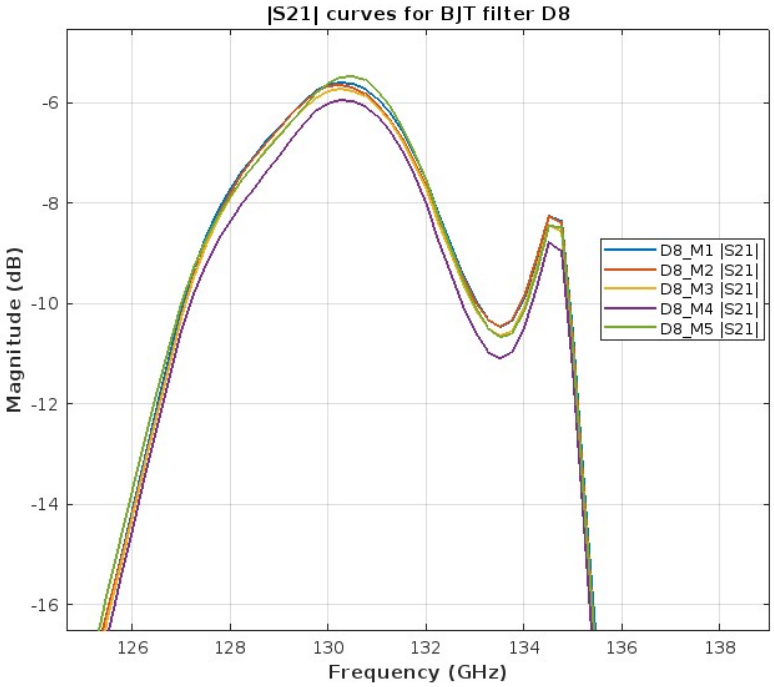

Figure 4.12: Loss magnitude and frequency deviations BJT filter D8.

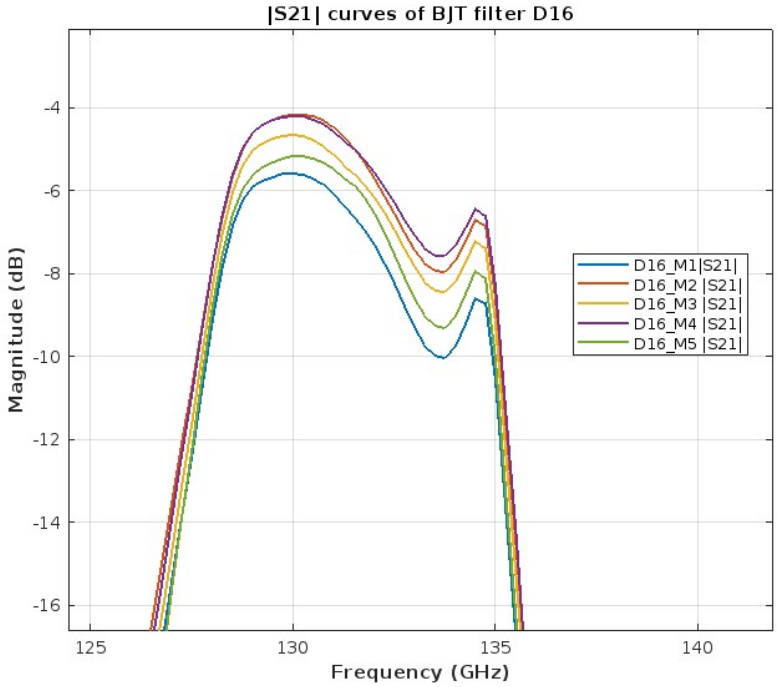

Figure 4.13: Loss magnitude and frequency deviations BJT filter D16.

4.2 Dimensional and Surface Analysis

Surface characterization and dimensional accuracy were measured using a 3D laser microscope and an optical microscope, respectively. Outer dimensions were measured for both filter types, and it was observed that there was a shrinkage range between 1-2%. These observations were with BJT filters. The E-Band and D-Band filters, whose peak frequencies and corresponding peak insertion loss magnitudes were close to the desired frequency and loss magnitude, were selected for outer dimension measurements as stated in 4.1, 4.2. Dimensional analysis on cross-sections showed that BJT cavity 4.14 widths were within +2.0% of nominal dimensions, whereas PBF-LB cavities undershot by 10%. Fin width in BJT 4.15 was within 0.7% of nominal dimension; PBF-LB fins were oversized by 101%, consistent with the S-parameters of the PBF-LB filters, which showed increased insertion loss and a reduced return-loss margin relative to the baseline, as illustrated in 4.6, 4.7.

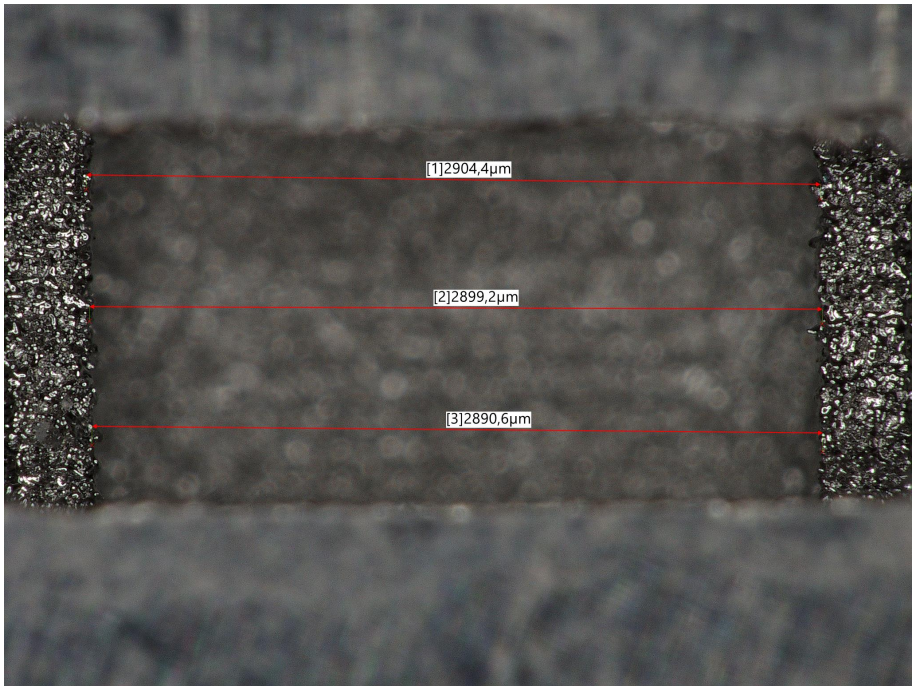

Figure 4.14: BJT E-Band, E5 cavity dimensions.

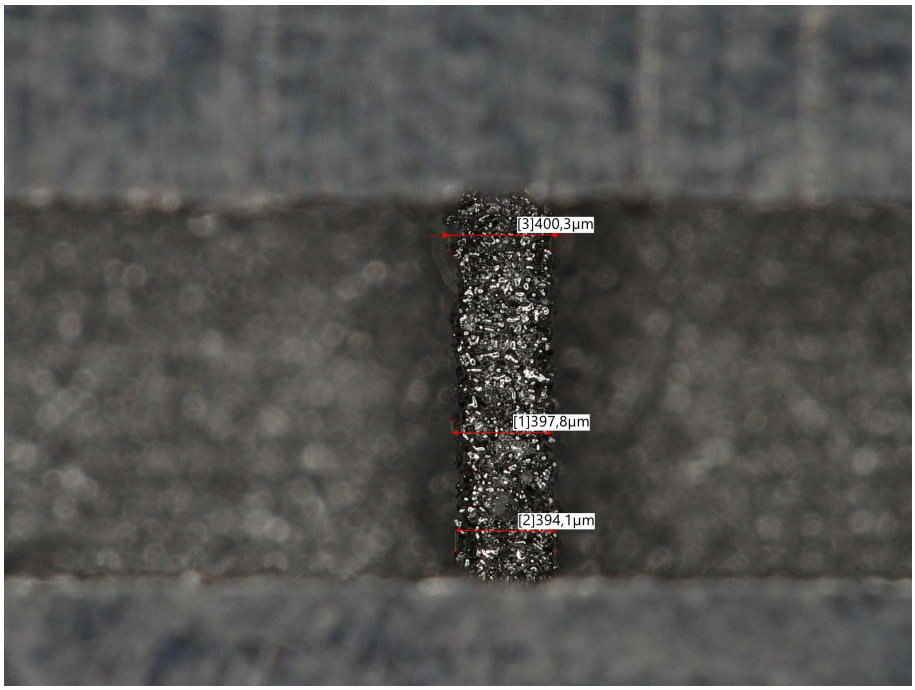

Figure 4.15: BJT E-Band, E5 fin dimensions.

Table 4.1: Outer Dimensions and Percentage Deviation from Nominal (16 × 3 × 4 mm) for BJT D-Band Filters

Filter	L (mm)	B (mm)	H (mm)	% Dev L	% Dev B	% Dev H
D1	15.71	2.89	3.99	-1.81%	-3.67%	-0.25%
D2	15.83	2.88	3.98	-1.06%	-4.00%	-0.50%
D4	15.82	2.89	3.98	-1.13%	-3.67%	-0.50%
D5	15.80	2.89	3.99	-1.25%	-3.67%	-0.25%
D18	15.82	2.90	4.00	-1.13%	-3.33%	0.00%
D20	15.88	2.89	4.00	-0.75%	-3.67%	0.00%
D11	15.77	2.90	4.00	-1.44%	-3.33%	0.00%
D12	15.91	2.90	3.98	-0.56%	-3.33%	-0.50%

Table 4.2: Outer Dimensions and Percentage Deviation from Nominal (32 × 6 × 8 mm) for Selected BJT E-Band Filters

Filter	L (mm)	B (mm)	H (mm)	% Dev L	% Dev B	% Dev H
E1	31.77	5.90	8.08	-0.72%	-1.67%	1.00%
E2	31.88	5.85	8.08	-0.38%	-2.50%	1.00%
E4	31.95	5.88	8.03	-0.16%	-2.00%	0.37%
E5	31.80	5.85	8.01	-0.62%	-2.50%	0.12%
E11	31.91	5.91	8.01	-0.28%	-1.50%	0.12%
E12	32.07	5.91	8.00	0.22%	-1.50%	0.00%
E18	31.86	5.87	8.02	-0.44%	-2.17%	0.25%
E20	31.90	5.87	8.01	-0.31%	-2.17%	0.12%

Table 4.3: Comparison of Measured Filter Cavity Dimensions with CAD Model

Sample	Avg. Measured (μm)	CAD Dimension (μm)	Deviation (%)
BJT Cavity	2898.07	2840	+2.04
SLM Cavity	2550.05	2840	-10.21

Table 4.4: Comparison of Measured Fin Widths with CAD Model

Sample	Avg. Measured (μm)	CAD Dimension (μm)	Deviation (%)
BJT Fin	397.4	400	-0.65
SLM Fin	805.5	400	+101.38

As discussed earlier in the report, the filters were split open in two orientations. The optical microscope Keyence VHX X1 was used to measure the internal fins and cavities. Both the profile and areal surface roughness were measured using the 3D laser confocal microscope Keyence VK-3000. The profile roughness is called the line roughness in the software, and the areal surface roughness is called the surface roughness. Three roughness parameters were selected: for profile Ra, Rz, Rms, and for areal roughness Sa, Sz, and Sq. ISO compliant roughness measurements were also explored. Profile roughness was measured for two E-Band filters, each of BJT and PBF-LB processes, by maintaining a sampling (cut-off) length λc of 2.5

mm. ISO-compliant traces (Table 4.7) were acquired at 2.5× so the field of view permitted an sampling length $\lambda_c = 2.5\,\text{mm}$. The 5× traces in Table 4.6 did not span the required sampling length and are therefore not ISO compliant. This difference in trace length also explains part of the variation observed in Ra between the two tables.

Table 4.5: Profile roughness measurement results for D-Band filters

Filter Name	AM Technology	Ra (µm)	Rz (µm)	Rsm (µm)
D14	BJT	12.620	79.555	168.501
D15	BJT	7.516	56.365	113.487
D1	BJT	11.304	78.588	132.475
D17	BJT	8.333	47.967	475.851
DR1 SLM	PBF-LB	11.536	63.646	131.762
DC5 SLM	PBF-LB	10.285	47.445	238.740

Table 4.6: Line roughness measurement results for E-Band filters

Filter Name	AM Technology	Ra (µm)	Rz (µm)	Rsm (µm)
E1	BJT	14.146	91.089	173.723
E3	BJT	11.224	90.200	224.469
E20	BJT	8.682	40.621	74.016
ER2 SLM	PBF-LB	5.778	43.905	118.334
EC3 SLM	PBF-LB	9.605	91.715	172.371
EB4 SLM	PBF-LB	15.424	102.990	184.962

Table 4.7: Line roughness measurement of E-Band filters (ISO compliant)

Filter Name	AM Technology	Ra (µm)	Rz (µm)	Rsm (µm)
EB4 SLM	PBF-LB	8.842	52.203	375.863
E1	BJT	9.451	64.996	244.120

Table 4.8: Areal Surface Roughness Parameters of E-Band Filters

Sample	AM Technology	S_a (μm)	S_z (μm)	S_q (μm)
E1	BJT	14.316	184.462	17.949
EB4 SLM	PBF-LB	16.708	109.537	19.818

4.3 Performance of Plated (ECP) filters

Both E-Band and D-Band filters underwent ECP. Five filters were chosen for E-Band - E2, E8, E12, E14, E15 and for D-Band - D2, D3, D5 , D6, D7. Electrical tests were performed for all the plated filters. Upon splitting of two filters of each band, it was

observed that plating was incomplete in E-Band as shown in 4.21, but in D-Band, plating was complete 4.20. Furthermore, the frequency vs loss magnitude plots in 4.16, 4.17, 4.18, 4.19 are comparison between filters before and after plating for both bands. Surface roughness measurements were performed for one plated filter. It was split in an orientation that would expose the fins along with the cavity.

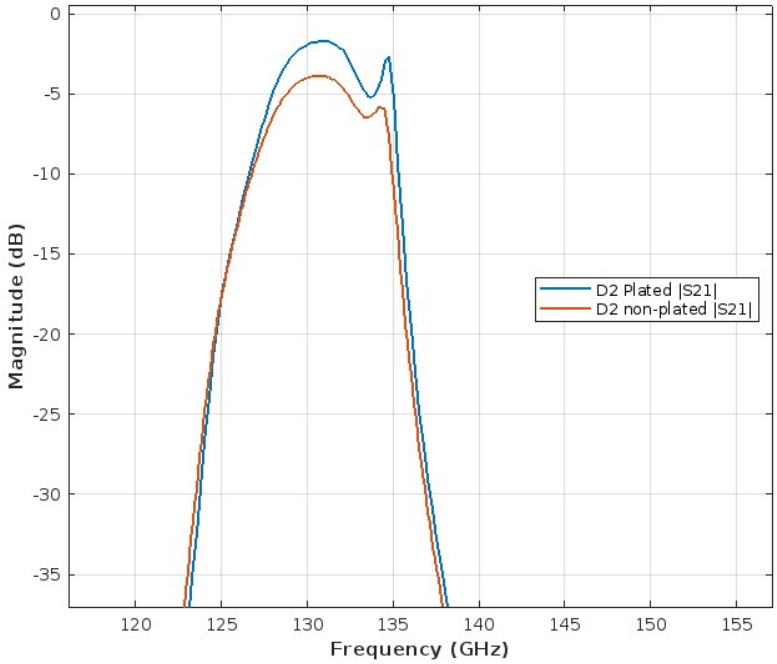

Figure 4.16: S21 comparison plot for D2 filter before and after plating.

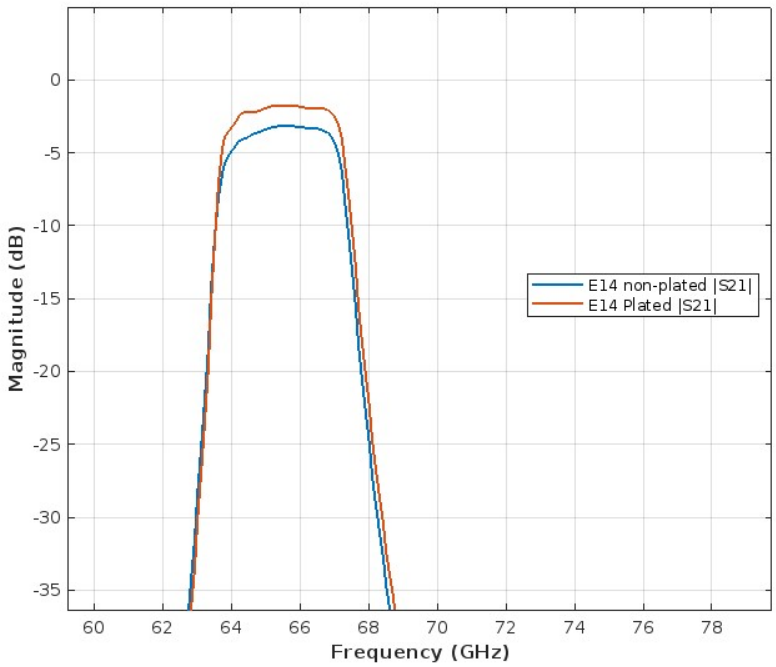

Figure 4.17: S21 comparison plot for E14 filter before and after plating.

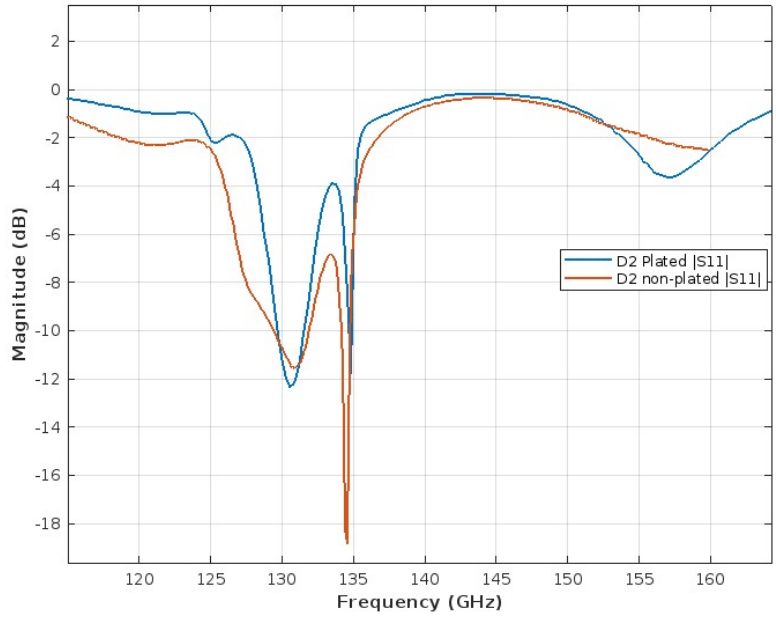

Figure 4.18: S11 comparison plot for D2 filter before and after plating.

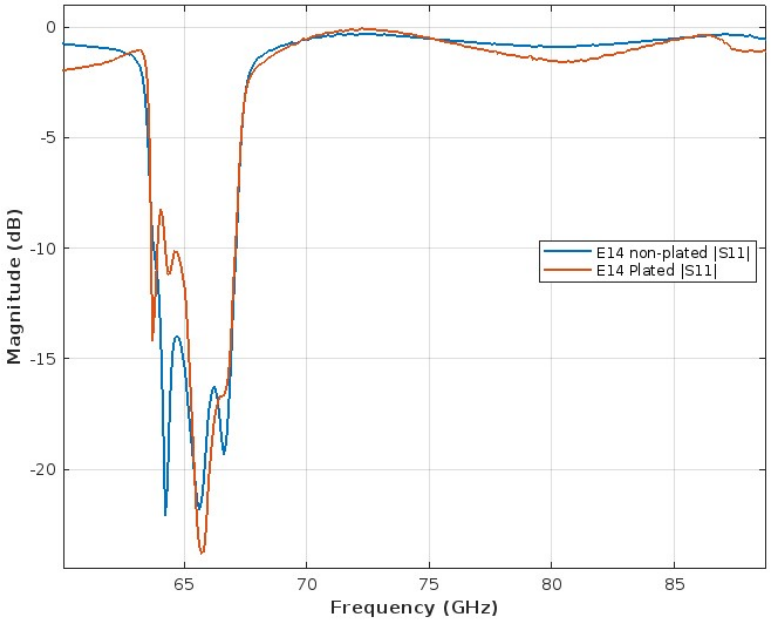

Figure 4.19: S11 comparison plot for E14 filter before and after plating.

Table 4.9: Peak Frequency and Magnitude for S21 Parameters

D Band	PeakFreq (GHz)	PeakMag (dB)
D2(Plated)	131	-1.6651
D-Band(Simulated)	132.1	-3.644
D2(Non-Plated)	130.7	-3.8281

Table 4.10: Peak Frequency and Magnitude for S21 Parameters (E14 Series)

E Band	PeakFreq (GHz)	PeakMag (dB)
E14(Non-plated))	65.6	-3.1242
E14(Plated))	65.5	-1.701

Table 4.11: Profile roughness measurement result for copper-plated filter E12

Filter Name	AM Technology	Ra (µm)	Rz (µm)	Rsm (µm)
E12	BJT	8.376	43.047	226.018

Figure 4.20: Split copper-plated D-Band filter.

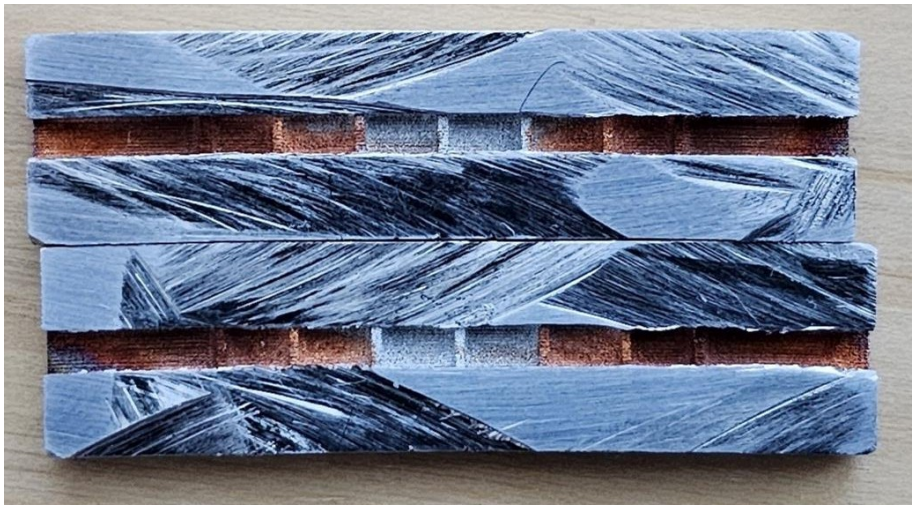

Figure 4.21: Split copper-plated E-Band filter.

5
Discussion

The idea behind this thesis was to evaluate which AM technology is best suitable to manufacture the microwave RF waveguide filters for E-Band and D-Band frequencies. The need for investigating AM technologies arose given the small dimensions (16 x 8 mm) and intricate internal features, and also to have a filter that does not have to be assembled and can be manufactured in one go. Another aim was to evaluate how the surface roughness of AM surfaces can influence the electrical performance and the frequency output. The material selection process was also stressed during this project. Copper or aluminum would have been ideal options for manufacturing the filters, but due to the unavailability of these materials, a more abundantly used material, SS316L, was used. Theoretically, LMM, BJT, MJT, and PBF-LB are most suitable for manufacturing the filters. However, BJT and PBF-LB were available for this project.

The next step after manufacturing the components was to assess the electrical VNA characterization of all the filters. This included comparing the actual performance of the manufactured filters with the simulated filters. In the case of BJT-manufactured filters, electrical tests show lower insertion loss compared to those of PBF-LB printed filters. The output frequency responses remained close to the magnitudes |S11| and |S22| <-15dB and |S12| >-0.6dB (E-band) >-1.0 dB (D-band) in the passband for both E-band and D-band filters,and the frequencies ranged between 65-67 GHz and 130-134GHz for E-band and D-band, respectively. The frequency vs magnitude plot A.11 of BJT D-band filter D3 shows that the insertion loss |S21| curve closely follows the simulated passband profile. However, the return loss |S11| of the simulated filter is more defined than that of the manufactured filter. There was not much shift in the output frequency upon testing all 20 E-band filters, which suggests repeatability in the same build. The dips and fluctuations in the |S11| curves potentially relate to the feedback from the fins and cavities within the internal structure. So, for instance, if the channel has six cavities, then there could be six fluctuations in the curve. This was observed in several E-band filters 4.2, 4.3, which further can be suggestive of the adequate internal geometries being met, ensuring better functionality of the component.

While the E-band filters showed promising results with output frequency being maintained within the required range and insertion loss lying close to the acceptable loss of -3 dB, it was equally important to evaluate the BJT printed parts for the D-band filters. In the case of D-Band filters, the |S21| curves were not as accurate as the simulated ones. However, some of the D-band filters showed adequate performance,

for example, in filters D6 and D3, the frequency band remained within the desired range of 130 134 GHz with lower insertion loss 4.4, 4.5. Based on the design, the filter is supposed to have six cavities, which would give six fluctuations in the |S11| curves. This was observed in the E-band as discussed above, but was not prominent in D-band filters. In a filter like D2, the fluctuations were less than six, which could potentially mean that the geometrical accuracy was not met adequately A.9. Furthermore, there were considerable fluctuations in the VNA tests due to poor contact with the waveguide flange in the test rigs. Necessary measures were taken in adjusting the fixtures by screwing them properly from both ends, and holding the filters in place. The small face of the filter caused inaccurate metal-to-metal contact, leading to measurement error. This is evident from the observed spread in the ||S21|| frequency response curves obtained from the VNA measurements.

The electrical VNA characterization of the PBF-LB manufactured filters for both E-band and D-band filters was also analyzed. There was significant insertion loss |S21| in both D-Band and E-Band filters 4.9, 4.7. The |S11| also showed increased losses 4.8, 4.6. This can be attributed to high surface roughness and inaccurate dimensions within the internal channel 4.5, 4.6. The presence of the |S21| curve at all means that there was a form of signal passability within the channels. There were fluctuations in the |S11|, especially in the case of E-Band filters, which suggests that there is some feedback from the cavities.

Because loss magnitudes and frequency outputs are typically dominated by the condition of the internal , the surface analysis prioritized those regions 2.1.1. For BJT, parts were scaled by 20% at the design stage to compensate for sinter shrinkage. Dimensional analysis indicated that internal dimensions were close to CAD, whereas outer dimensions were smaller by approximately 1–2% 4.6 when measured with a digital caliper (accuracy ± 0.02 mm). Local deviations of the outer profile were observed visually; however, the extent could not be quantified reliably because large-area optical stitching was not available. To expose the internal channel for dimensional and surface analysis, filters were split along two orthogonal planes. The diamond saw produced both halves but introduced protrusions on the cut faces. Although milling yielded single-sided sections cleaner than the saw, protrusions into the cavities were still observed and had to be removed manually. Despite careful removal of these artefacts, residual features reduced the accessible measurement area and biased placement toward smoother, unobstructed regions. The measurements were conducted after removing as many uneven protrusions as possible. Therefore, the measurements were performed under conditions of minimal interference from the remaining uneven protrusions. The uneven protrusions also limit the area of the internal channel, which can be evaluated for both dimensional and surface roughness measurements.

Profile and areal surface roughness were measured for both PBF-LB-manufactured filters and BJT parts. The aim was to evaluate the AM surfaces within the filters and draw conclusions on their relation to the overall performance of the filters. For ensuring reliability and repeatability of roughness values ISO adherence is useful.

ISO standard length could not be followed for all the filters due to the smaller size of the components, especially the internal channels with dimensions of 0.4 mm and 2.840 mm. One instance is that a sampling length of 2.5 mm was utilized so as to have a standard measurement to validate the results. An area of 2 x 2 mm was tried to be scanned for a reliable result, which was feasible in one orientation and in E-Band filters pertaining to its larger size. The intent was to determine the overall roughness of the AM surfaces. As shown in A.3, the Ra values of PBF-LB were observed to be lower than those of BJT filters. However, when it comes to electrical performance, BJT filters have better loss magnitudes and frequency output than PBF-LB filters.

The electroless copper plating aimed at potentially increasing the electrical performance, subsequently enhancing the frequency output of the filters. Even though the plating did not reach the middle cavities and the fins, as shown in 4.21 of filter E14 within the internal channel, functionality-wise, they still performed better than the non-plated filters. The plating was complete in the D-Band filter. Electrical characterization showed a reduction in loss magnitude, and the passband remained within the target range. In the case of the D-band filter, the loss magnitude of AM-manufactured filters turned out to be higher than the simulated results. For instance, copper-plated D2 filters gave a loss magnitude of -1.67 dB, whereas a simulated D-band filter gave a loss magnitude of -3.64 dB. Though simulation was carried out for D-Band SS316L material but the surface was assumed to be smooth and not textured like AM surfaces. This is quite promising for future additively manufactured filters. Printing defects were observed in both AM processes. Since the defect in the PBF-LB component was on the outer edge of the filter, it did not affect its functionality. However, in the case of BJT, the defect was detected only when electrical testing was carried out. With a loss magnitude as high as -21 dB in BJT filter D12, it was evident that the filter had a defect. This was confirmed by splitting the same filter open, and it was observed that material was sticking inside the internal cavity.

The design of the waveguide filter focuses primarily on its mechanical and electrical characteristics and was designed for milling. Any alterations in the design of the component can impact the filter's performance. Furthermore, from a DFAM perspective, the components would require alterations based on factors such as orientation, support structures.

6
Conclusion

This thesis investigated the feasibility of utilizing AM to produce high-frequency waveguide filters operating in the E-Band (65–67 GHz) and D-Band (130–134 GHz). Among the AM technologies, BJT and PBF-LB were the two processes that were employed for manufacturing the filters. The study was motivated by the increasing demand for high-performance RF components in future communication systems and the adoption of sustainable manufacturing practices that align with Ericsson's 2030 neutrality target.

The experimental results show that the most suitable AM process for manufacturing the waveguide filter structure of this complexity is BJT. BJT produced filters exhibited lower surface roughness, more consistent geometries and gave better overall results compared to PBF-LB components. Although D-Band filters were more challenging due to their reduced geometric sizes, the functional performance of the selected BJT components was within acceptable limits. The dimensional analysis tracked the accuracy of the critical internal features and the ability to plate those features. BJT parts held fin and cavity dimensions close to nominal (fin $-0.65\,\%$, cavity $+2.04\,\%$), while PBF-LB exhibited large deviations (fin $+101\,\%$, cavity $-10.21\,\%$); the latter correlated with high insertion loss. Where internal copper coverage was complete D-band, insertion loss decreased and even undercut the smooth-wall SS316L simulation ($\sim 3.64\,\mathrm{dB}$). In E-Band, plating did not reach mid-cavities and fins; improvements were smaller. These findings indicate that dimensional accuracy of fins/iris and cavity span, together with assured plating reach, are the dominant levers for manufacturability and RF performance at these bands.

In contrast, PBF-LB components showed limited electrical functionality and high insertion loss due to deviations in the dimensions within the internal cavities and fins. Electroless Copper Plating resulted in partial improvements in electrical performance, particularly for BJT filters. However, non-uniform plating within the internal channels in E-Band filters limited their overall effectiveness. In conclusion, BJT currently offers viability for the additive manufacturing of complex, high-frequency RF filters. The filters will require further optimization in terms of AM process parameters, DFAM, and post-treatment techniques.

7
Future Work

Future research will need to investigate copper-based AM. Although BJT has offered great possibilities to fabricate high-frequency RF filters with complex internal geometry, further improvement of material selection, and surface treatment. DFAM can play a critical role in closing the performance gap with traditionally machined components. With this approach, the filter design can be modified by considering process limitations and post-processing needs. For example, the internal pathways can be redesigned or an inconspicuous drain can be added to allow uniform plating.

During the electrical testing in this project, issues occured from inaccurate contact between the printed filters and the testing rig, which introduced uncertainty into the measured S-parameters. This highlights the importance of sample preparation and interface design in both the development and validation stages. Future designs could incorporate modifications to ensure consistent, repeatable fixture contact, such as slightly enlarging the external footprint of the filter while preserving the internal channel geometry. These changes would ensure stability and repeatability in measurements. Exploration of other AM technologies, such as LMM and MJT, could be considered, especially for copper or other better electrically conductive materials. As highlighted in the project, AM surface analysis is also important; therefore, alternative cutting operations such as Electrical Discharge Machining instead of milling or using a diamond cutting machine could be considered to obtain better cross-sections of the parts for surface characterization in future studies.

Bibliography

[1] Aziz Ul Hassan Mohsan and Dongbin Wei. Advancements in additive manufacturing of tantalum via the laser powder bed fusion (pbf-lb/m): A comprehensive review. *Materials*, 16(19), 2023.

[2] W. Sha, X. Wu, and K.G. Keong. 1 - introduction to electroless copper and nickel–phosphorus (ni–p) depositions. In W. Sha, X. Wu, and K.G. Keong, editors, *Electroless Copper and Nickel–Phosphorus Plating*, Woodhead Publishing Series in Metals and Surface Engineering, pages 1–12. Woodhead Publishing, 2011.

[3] Ericsson. Microwave transport — mini-link 6000, 2025. Accessed: 2025-06-27.

[4] everythingRF. Microwave and rf filters, 2025. Accessed: 2025-06-27.

[5] Mini-Circuits. Waveguide filters, 2025. Accessed: 2025-06-27.

[6] Yunfeng Dong, Tom K Johansen, Vitaliy Zhurbenko, and Öncel Acar. Design procedure for compact folded waveguide filters. In *2015 1st URSI Atlantic Radio Science Conference (URSI AT-RASC)*. IEEE, May 2015.

[7] Raghavendra G Kulkarni. Fields inside a waveguide: A different approach [educator's corner]. *IEEE Microw. Mag.*, 25(4):110–112, April 2024.

[8] Jeffrey Hesler. A gold rush to d-band and beyond. *Electronics World*, 128(2030):33 – 34, 2023. Cited by: 0.

[9] Ericsson. Spectrum in a dynamic market, 2022. Accessed: 2025-05-30.

[10] RI.SE. Ericsson looking to move from research to production, 2022. Accessed: 2025-05-30.

[11] D. Kim, J. Park, and H. Lee. Impact of surface roughness on high-frequency electromagnetic wave propagation in additive manufactured waveguide filters. *IEEE Transactions on Components, Packaging and Manufacturing Technology*, 14(2):123–132, 2024.

[12] Mauro Lumia, Giuseppe Addamo, Oscar Antonio Peverini, Flaviana Calignano, Giuseppe Virone, and Diego Manfredi. Additive manufacturing of rf waveguide components. In *Recent Microwave Technologies*. IntechOpen, 2022.

[13] Yang Yu, Yi Wang, Talal Skaik, Thomas Starke, Xiaobang Shang, Michael J. Lancaster, Peter Hunyor, Peter G. Huggard, Hui Wang, Michael Harris, Mat Beardsley, and Qingsha S. Cheng. D-band waveguide diplexer fabricated using micro laser sintering. *IEEE Transactions on Components, Packaging and Manufacturing Technology*, 12(9):1446–1457, 2022.

[14] Eduardo A. Rojas-Nastrucci, Justin T. Nussbaum, Nathan B. Crane, and Thomas M. Weller. Ka-band characterization of binder jetting for 3-d printing of metallic rectangular waveguide circuits and antennas. *IEEE Transactions on*

Microwave Theory and Techniques, 65(9):3099–3108, 2017. Accessed: 2025-05-29.

[15] Cheshta Kwatra, Kapil Gupta, Kshitij Chhabra, and Priyanka Jain. Design and implementation of microstrip low pass filter at 2.4 ghz. page 112 – 115, 2020.

[16] C. Camacho-Peñalosa and J.D. Baños-Polglase. On the definition of return loss. *IEEE Antennas and Propagation Magazine*, 55(2):172 – 174, 2013.

[17] Rohde & Schwarz. Understanding s-parameters. `https://www.rohde-schwarz.com/us/products/test-and-measurement/essentials-test-equipment/spectrum-analyzers/understanding-s-parameters_257831.html`. Accessed: 2025-08-12.

[18] Klas Eriksson. Personal communication. Ericsson, 2025. Personal communication.

[19] Thanh Do. Personal communication. Ericsson, 2025. Personal communication.

[20] RF Wireless World. Waveguide basics: Types, propagation modes, advantages & disadvantages. `https://www.rfwireless-world.com/tutorials/waveguide-basics/waveguide-basics`, 2025. Accessed: 2025-05-29.

[21] Ian Gibson, David Rosen, Brent Stucker, and Mahyar Khorasani. *Additive Manufacturing Technologies*. Springer, Cham, Switzerland, 3rd edition, 2021.

[22] International Organization for Standardization. ISO 17296-2:2016 – Additive manufacturing – General principles – Part 2: Overview of process categories and feedstock. `https://www-sis-se.eu1.proxy.openathens.net/en/produkter/manufacturing-engineering/additive-manufacturing/sseniso1729622016/`, 2016. Accessed: 2025-07-06.

[23] György Attila Harakály, Santiago Cano Cano, Johannes Bosters, Christian Gierl-Mayer, and Gerald Mitteramskogler. The applicability of lithography-based metal manufacturing for 316L stainless steel. In *Euro PM2023 Proceedings*. EPMA, September 2023.

[24] Sharlotte Kramer, Jennifer L Jordan, Helena Jin, Jay Carroll, and Alison M Beese, editors. *Mechanics of additive and advanced manufacturing, volume 8*. Conference proceedings of the Society for Experimental Mechanics. Springer International Publishing, Cham, Switzerland, 1 edition, August 2018.

[25] T. Studnitzky, K. Reuter, M. Altmann, A. Straub, Florian Häslich, O. Andersen, J. Scheibler, and T. Weißgärber. Stereolithography of copper for 5g, 6g and beyond. 2022. Cited by: 0.

[26] Francisco Werley Cipriano Farias, Telmo Jorge Gomes dos Santos, and João Pedro Oliveira. Directed energy deposition + mechanical interlayer deformation additive manufacturing: a state-of-the-art literature review. *Int. J. Adv. Manuf. Technol.*, 131(3-4):999–1038, March 2024.

[27] Francesco Careri, Stano Imbrogno, Moataz M Attallah, Khamis Essa, and Domenico Umbrello. Finite element modeling of machining nickel superalloy produced by direct energy deposition process. *Procedia Manuf.*, 47:525–529, 2020.

[28] Christoph Klahn and Bastian Leutenecker-Twelsiek. Design guidelines. In *Springer Handbook of Additive Manufacturing*, pages 177–198. Springer International Publishing, Cham, 2023.

[29] Chanun Suwanpreecha and Anchalee Manonukul. A review on material extrusion additive manufacturing of metal and how it compares with metal injection moulding. *Metals*, 12(3), 2022.

[30] Eujin Pei, Alain Bernard, Dongdong Gu, Christoph Klahn, Mario Monzón, Maren Petersen, and Tao Sun, editors. *Springer Handbook of Additive Manufacturing*. Springer, Cham, 2023. Accessed: 2025-05-29.

[31] Iacopo Bianchi, Archimede Forcellese, Pietro Forcellese, Tommaso Mancia, Chiara Mignanelli, Michela Simoncini, and Tommaso Verdini. Effect of printing orientation angle and heat treatment on the mechanical properties and microstructure of binder-jetting-printed parts in 17-4 ph stainless steel. *Metals*, 14(11):1220, 2024.

[32] K. Myers, A. Paterson, T. Iizuka, and A. Klein. The effect of print speed on surface roughness and density uniformity of parts produced using binder jet 3d printing. page 122 – 133, 2019. Cited by: 13.

[33] Erika Tuneskog, Karl-Johan Nogenmyr, Daniel Moell, Marcus Gullberg, and Lars Nyborg. Exploring surface roughness effects on spray performance in metal additive manufactured fuel injectors for gas turbine applications. *J. Jpn. Soc. Powder Powder Metall.*, 72(Supplement):S1233–S1239, March 2025.

[34] Ivan Aiza, Chiara Baldi, Federico Matías de la Vega, Sara Sebastiani, Niccolò Enrico Veronese, Mohammad Yousefi, Mohammad Hossein Mosallanejad, Erfan Maleki, Mario Guagliano, Luca Iuliano, Abdollah Saboori, and Sara Bagherifard. Effects of build orientation and inclined features on physical, microstructural and mechanical properties of powder bed fusion additively manufactured metallic parts. *Progress in Materials Science*, 147:101357, 2025.

[35] Didunoluwa Obilanade, Christo Dordlofva, and Peter Törlind. Surface roughness considerations in design for additive manufacturing – a literature review. In *Proceedings of the Design Society: 23rd International Conference on Engineering Design (ICED21)*, pages 2841–2850. Cambridge University Press, 2021.

[36] Erika Tuneskog, Lars Nyborg, and Karl-Johan Nogenmyr. Assessment of surface roughness in additively manufactured channels for fluid applications. In *Euro PM2024 Proceedings*. EPMA, October 2024.

[37] Jakub Sorocki, Ilona Piekarz, Michal Baranowski, Adam Lamecki, Alberto Cattenone, Stefania Marconi, Gianluca Alaimo, Nicolo Delmonte, Lorenzo Silvestri, and Maurizio Bozzi. Low-cost method for internal surface roughness reduction of additively manufactured all-metal waveguide components. *IEEE Trans. Microw. Theory Tech.*, 72(8):4519–4529, August 2024.

[38] Incus GmbH. Lithography-based metal manufacturing (lmm) technology. `https://www.incus3d.com/technology/`, 2025. Accessed: 2025-05-29.

[39] Nesma T. Aboulkhair, Federico Bosio, Negar Gilani, Chinmay Phutela, Richard J.M. Hague, and Christopher J. Tuck. Chapter six - additive manufacturing processes for metals. In Javad Kadkhodapour, Siegfried Schmauder, and Felix Sajadi, editors, *Quality Analysis of Additively Manufactured Metals*, pages 201–258. Elsevier, 2023.

[40] T. D. Ngo, A. Kashani, G. Imbalzano, K. T. Nguyen, and D. Hui. Additive manufacturing (3d printing): A review of materials, methods, applications and challenges. *Composites Part B: Engineering*, 143:172–196, 2018.

[41] Andrew Townsend, Nicola Senin, Liam Blunt, Richard K. Leach, and John S. Taylor. Surface texture metrology for metal additive manufacturing: a review. *Precision Engineering*, 46:34–47, 2016.

[42] Erika Tuneskog. Characterizing and modelling of surface roughness and its impact on additively manufactured fluid components, 2024.

[43] International Organization for Standardization. ISO 25178-2:2021 – Geometrical product specifications (GPS) – Surface texture: Areal – Part 2: Terms, definitions and surface texture parameters. `https://www.iso.org/standard/74696.html`, 2021. Second edition, published December 2021.

[44] International Organization for Standardization. ISO 25178-603:2025 – Geometrical product specifications (GPS) – Surface texture: Areal – Part 603: Design and characteristics of non-contact (phase shifting interferometry) instruments. `https://www.iso.org/standard/87669.html`, 2025. First edition, scheduled publication 2025.

[45] International Organization for Standardization. ISO 21920-1:2021 – Geometrical product specifications (GPS) – Surface texture: Profile – Part 1: Indication of surface texture. `https://www.iso.org/standard/74178.html`, 2021. First edition, published December 2021.

[46] International Organization for Standardization. ISO 21920-2:2021 – Geometrical product specifications (GPS) – Surface texture: Profile – Part 2: Terms, definitions and surface texture parameters. `https://www.iso.org/standard/74179.html`, 2021. First edition, published December 2021. Corrected version: June 2022.

[47] International Organization for Standardization. ISO 21920-3:2021 – Geometrical product specifications (GPS) – Surface texture: Profile – Part 3: Specification operators. `https://www.iso.org/standard/74180.html`, 2021. First edition, published December 2021.

[48] Wevolver. Comparison of contact vs non-contact surface metrology techniques, n.d.

[49] Taylor Hobson Centre of Excellence. Cut-offs and the measurement of surface roughness.

[50] Mike Mills. Cut-offs and the measurement of surface roughness. Technical report, Taylor Hobson, 2002. Accessed: 2025-05-29.

A

Appendix 1

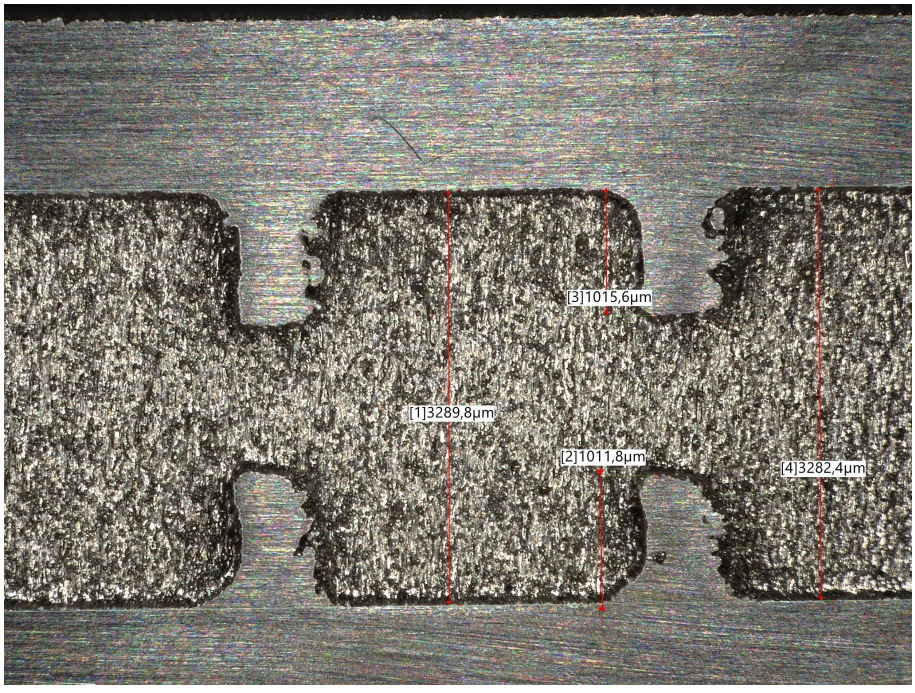

Figure A.1: Dimensions of cavity in PBF-LB E band filter.

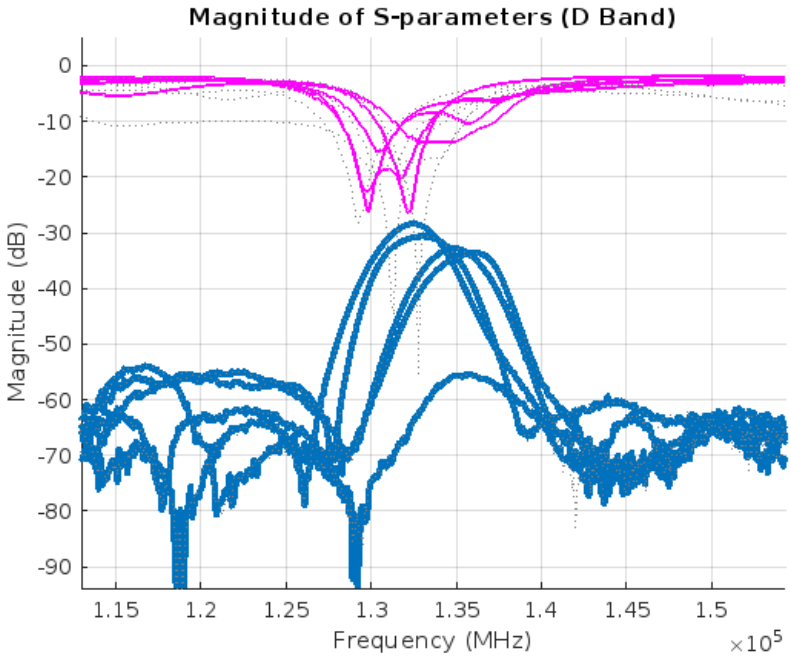

Figure A.2: PBF-LB, D band frequency vs magnitude plots.

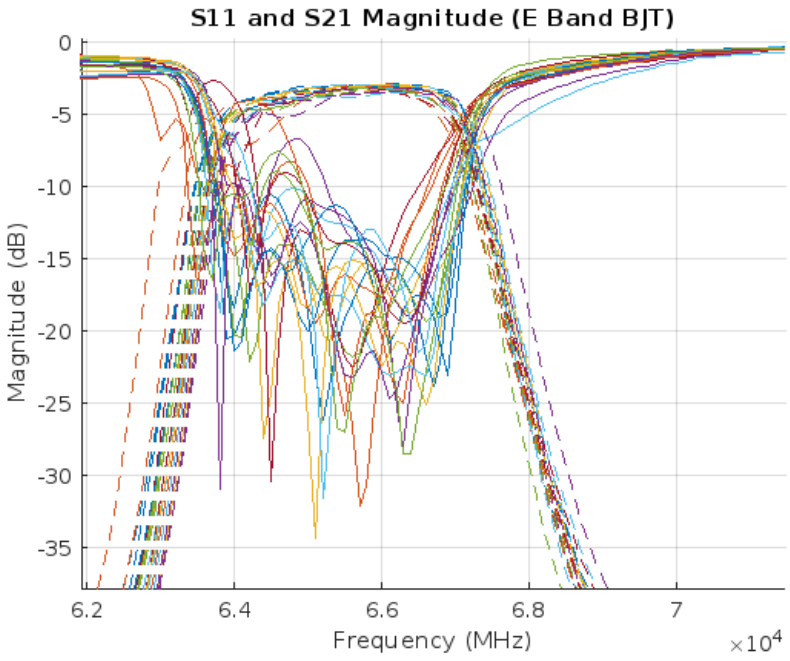

Figure A.3: BJT, E band frequency vs magnitude plots.

Surface roughness measurement D1B_SURFACE_5X KEYENCE VK-X3000 Series

Main image

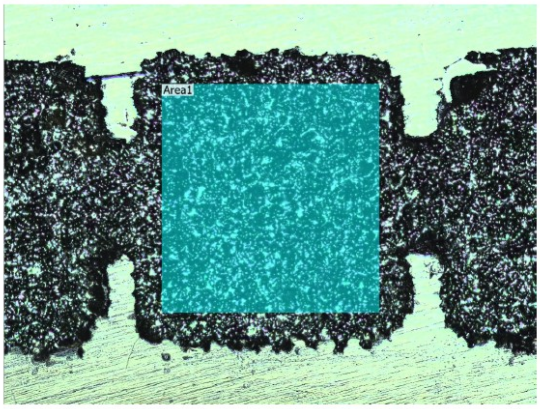

Scale-limited surface

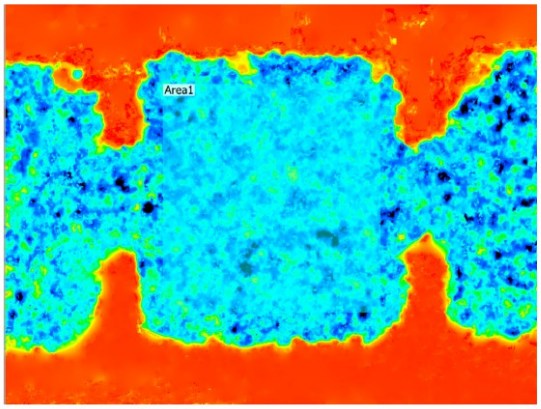

Analysis condition

Roughness standard	ISO 25178-2:2012
Filter type	Gaussian
S-filter	None
F-operation	None
L-filter	None
End effect correction	Enabled

Measurement result

	Sa	Sz	Sq
	µm	µm	µm
Max.	18,789	246,164	25,672
Min.	18,789	246,164	25,672
Ave.	18,789	246,164	25,672
Std. DV	0,000	0,000	0,000
Area1	18,789	246,164	25,672

Measured date : 2025-06-11 13:01:27
Objective Lens Power : 5X

Figure A.4: D1 filter areal surface roughness.

Surface roughness measurement E1_A_2.5N0.8 KEYENCE VK-X3000 Series

Main image

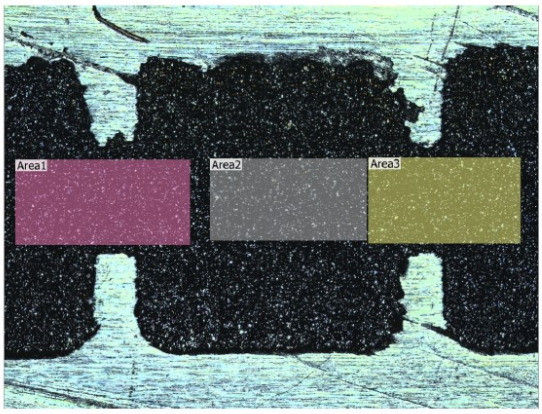

Scale-limited surface

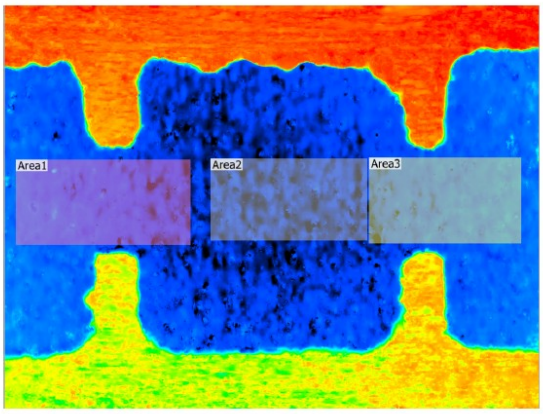

Analysis condition

Roughness standard	ISO 25178-2:2012
Filter type	Gaussian
S-filter	None
F-operation	None
L-filter	None
End effect correction	Enabled

Measurement result

	Sa	Sz	Sq
	µm	µm	µm
Max.	18,739	218,888	22,955
Min.	8,861	157,026	11,742
Ave.	14,316	184,462	17,949
Std. DV	4,098	25,734	4,656
Area1	18,739	218,888	22,955
Area2	8,861	157,026	11,742
Area3	15,347	177,472	19,151

Measured date : 2025-06-11 11:38:51
Objective Lens Power : 2,5X

Figure A.5: E1 filter areal surface roughness.

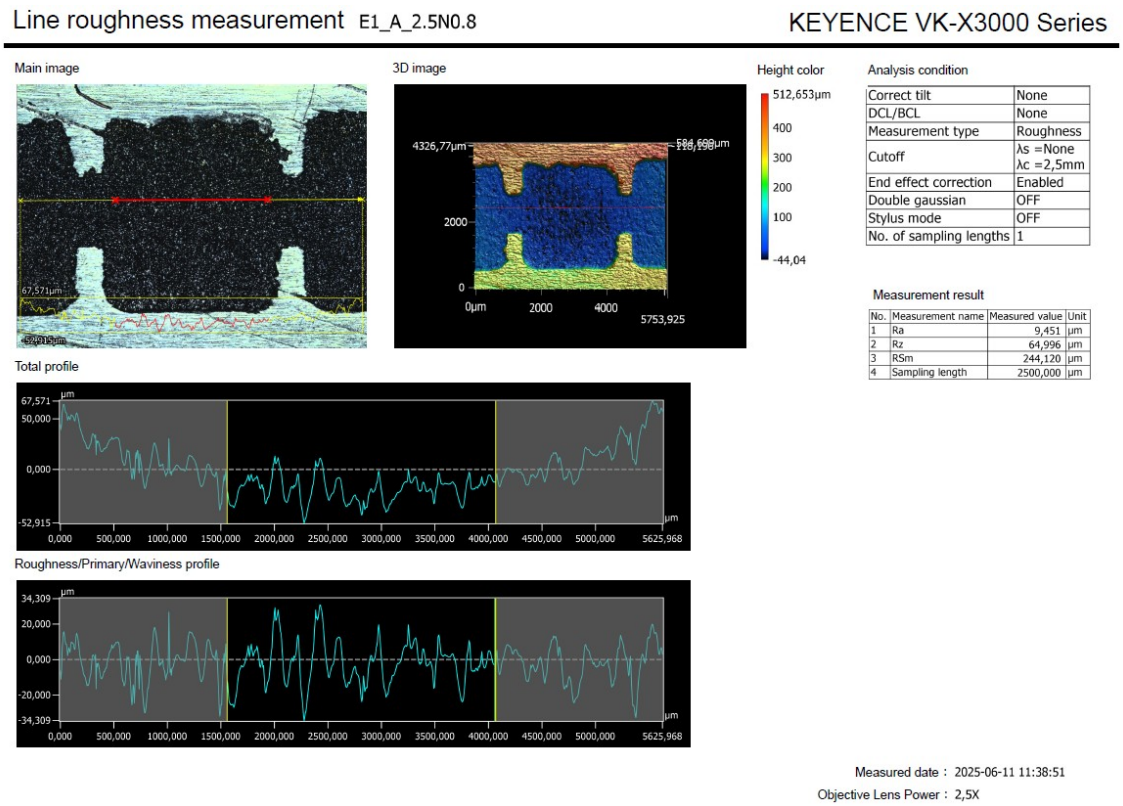

Figure A.6: E1 filter profile surface roughness.

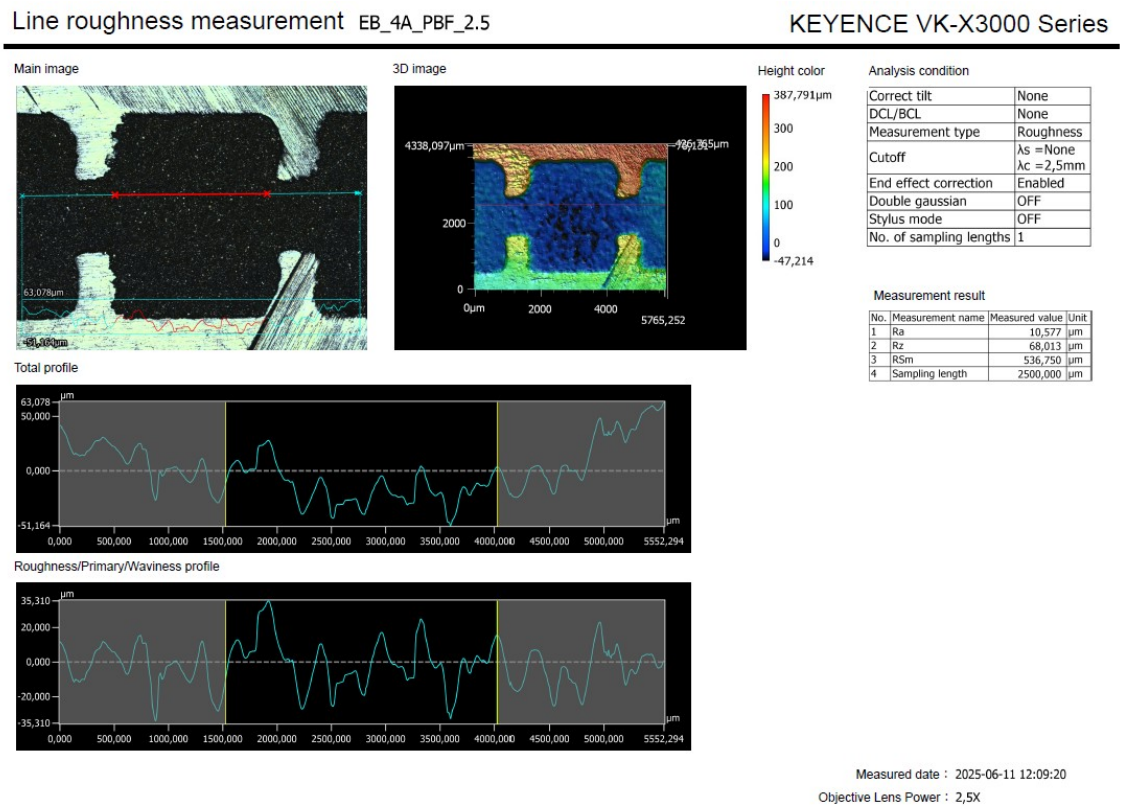

Figure A.7: EB4 SLM filter profile surface roughness.

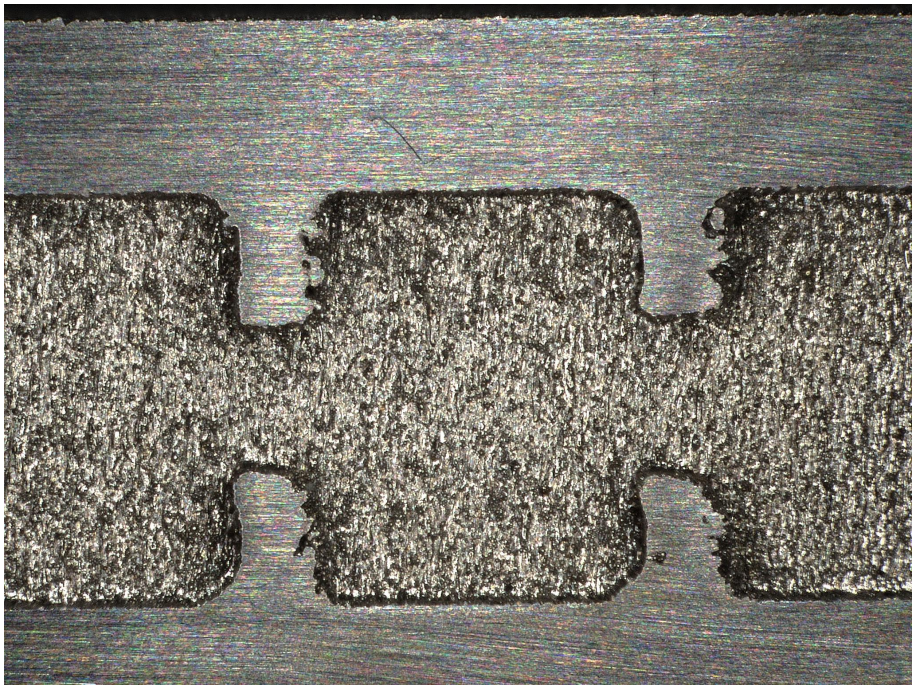

Figure A.8: PBF - LB manufactured E-band filter surface texture.

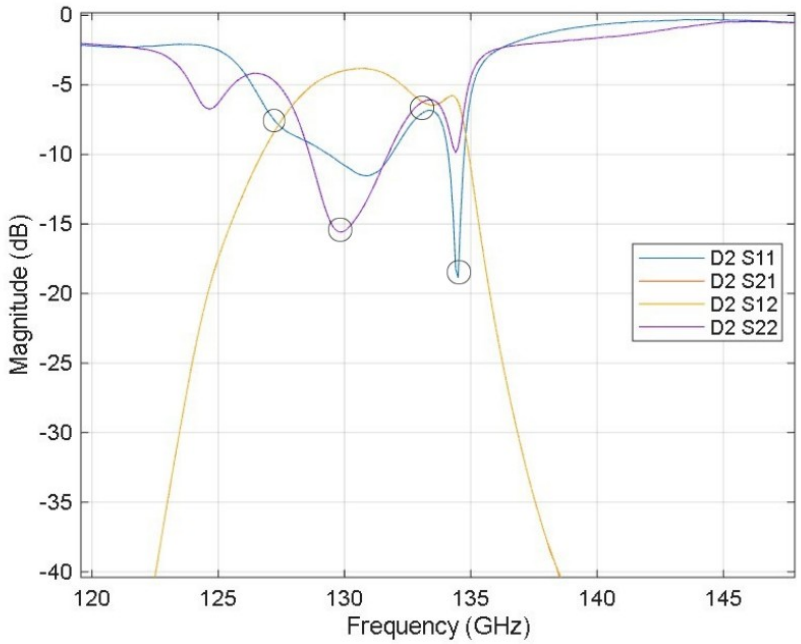

Figure A.9: Fluctuations on S11 curve in D2 filter highlighted with black circles.

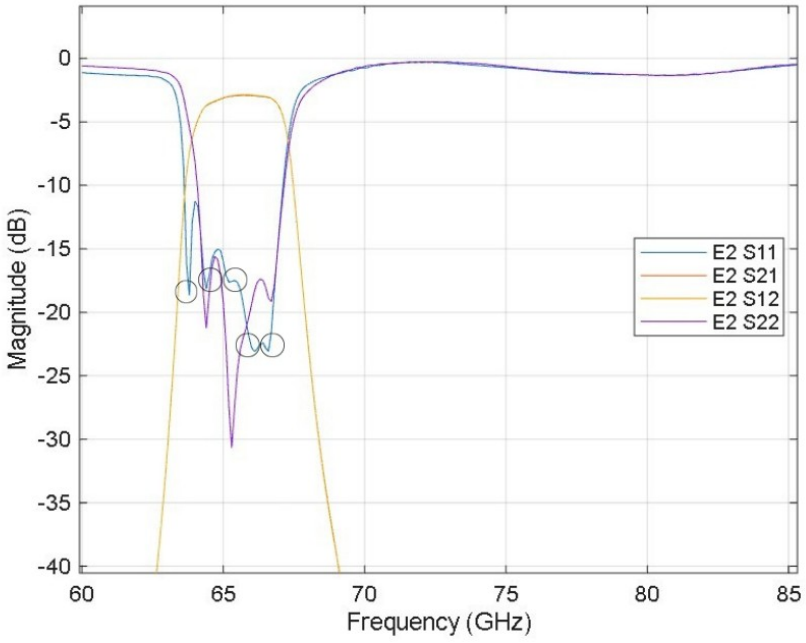

Figure A.10: Fluctuations on S11 curve in E2 filter highlighted with black circles.

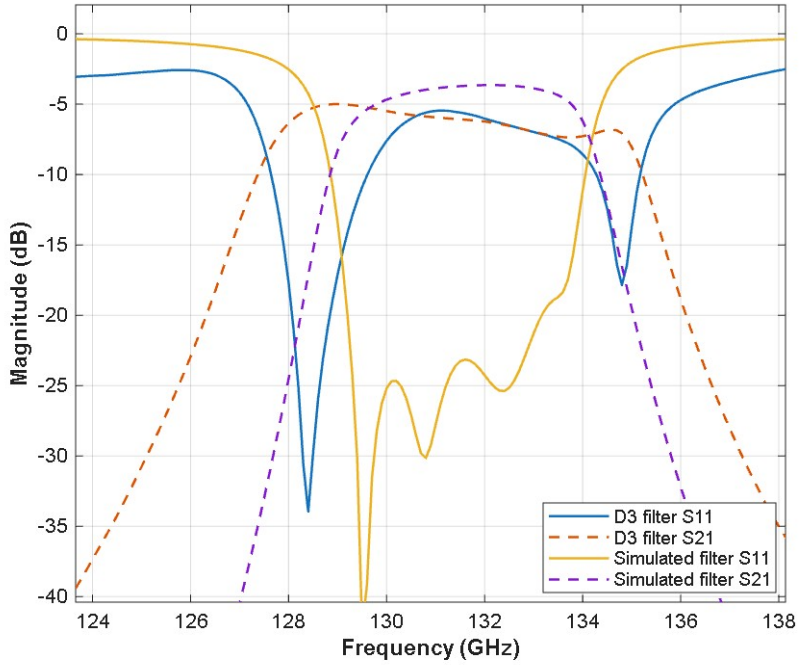

Figure A.11: Simulated filter vs manufactured D-band D3 filter

Table A.1: Waveguide Specifications: Frequency Range and Inner Dimensions (in mm)

Waveguide Name	**Recommended Frequency**	**A [mm]**	**B [mm]**
WR28	26.50 – 40 GHz	7.112	3.556
WR22	33.00 – 50 GHz	5.6896	2.8448
WR19	40.00 – 60 GHz	4.7752	2.3876
WR15	50.00 – 75 GHz	3.7592	1.8796
WR12	60.00 – 90 GHz	3.0988	1.5494
WR10	75.00 – 110 GHz	2.54	1.27
WR8	90.00 – 140 GHz	2.032	1.016
WR6	110.00 – 170 GHz	1.651	0.8255
WR5	140.00 – 220 GHz	1.2954	0.6477
WR4	172.00 – 260 GHz	1.0922	0.5461

Table A.2: Test matrix for manufactured filters

Filter Name	AM Technology	Electrical Characterization	Surface Analysis	Dimensional Analysis	Plating
D1	BJT	Yes	Yes	Yes	
D2	BJT	Yes			Yes
D3	BJT	Yes			Yes
D4	BJT	Yes			
D5	BJT	Yes			Yes
D6	BJT	Yes			Yes
D7	BJT	Yes			Yes
D8	BJT	Yes			
D9	BJT	Yes			
D10	BJT	Yes			
D11	BJT	Yes			
D12	BJT	Yes	Yes		
D13	BJT	Yes			
D14	BJT	Yes	Yes		
D15	BJT	Yes	Yes		
D16	BJT	Yes			
D17	BJT	Yes	Yes		
D18	BJT	Yes			
D19	BJT	Yes			
D20	BJT	Yes			
E1	BJT	Yes	Yes		
E2	BJT	Yes			Yes
E3	BJT	Yes	Yes	Yes	
E4	BJT	Yes			
E5	BJT	Yes			
E6	BJT	Yes			
E7	BJT	Yes			
E8	BJT	Yes			Yes
E9	BJT	Yes			
E10	BJT	Yes			
E11	BJT	Yes			
E12	BJT	Yes	Yes		Yes
E13	BJT	Yes			
E14	BJT	Yes			Yes
E15	BJT	Yes			Yes
E16	BJT	Yes			
E17	BJT	Yes			
E18	BJT	Yes			
E19	BJT	Yes			
E20	BJT	Yes	Yes		
D R1 SLM	PBF-LB	Yes	Yes		
D U2 SLM	PBF-LB	Yes			
D B3 SLM	PBF-LB	No			
D L4 SLM	PBF-LB	No			
D C5 SLM	PBF-LB	Yes			
E U1 SLM	PBF-LB	Yes			
E R2 SLM	PBF-LB	Yes	Yes		
E C3 SLM	PBF-LB	No	Yes		
E B4 SLM	PBF-LB	No	Yes	Yes	
E L5 SLM	PBF-LB	Yes			

Table A.3: Summary of electrical peaks and surface roughness metrics for all filters

Filter Name	**Peak S21** (dB)	**Peak S11** (dB)	**Peak Frequency** (GHz)	**Sa** (μm)	**Sz** (μm)	**Sq** (μm)	**Ra** (μm)	**Rz** (μm)	**Rsm** (μm)
D1	-5.59	-24.0	132.1	18.78	246.16	-	11.30	78.58	132.47
D2	-3.82	-18.84	130.7	-	-	-	-	-	-
D3	-4.99	-33.97	129	-	-	-	-	-	-
D4	-6.44	-10.90	131.5	-	-	-	-	-	-
D5	-4.87	-20.31	132.1	-	-	-	-	-	-
D6	-5.23	-27.52	130.7	-	-	-	-	-	-
D7	-5.46	-34.32	130.9	-	-	-	-	-	-
D8	-5.68	-8.99	130.3	-	-	-	-	-	-
D9	-7.29	-11.35	131.3	-	-	-	-	-	-
D10	-5.19	-14.04	131.6	-	-	-	-	-	-
D11	-4.66	-17.33	133.1	-	-	-	-	-	-
D12	-21.7	-3.17	130.1	-	-	-	-	-	-
D13	-10.63	-7.55	128	-	-	-	-	-	-
D14	-5.56	-12.57	131.3	-	-	-	12.62	79.55	168.50
D15	-4.21	-19.85	133.4	8.84	104.21	-	7.51	56.36	113.49
D16	-4.34	-16.21	129.9	-	-	-	-	-	-
D17	-5.01	-12.11	131.3	-	-	-	8.33	47.96	-
D18	-3.91	-26.97	130.1	-	-	-	-	-	-
D19	-6.23	-19.0	131.6	-	-	-	-	-	-
D20	-4.68	-22.19	131.6	-	-	-	-	-	-
E1	-3.42	-27.99	66.1	14.31	184.46	17.95	14.14	91.09	173.72
E2	-2.90	-23.09	65.7	-	-	-	-	-	-
E3	-3.02	-19.47	66.1	-	-	-	11.22	90.20	224.47
E4	-3.0	-23.05	66.1	-	-	-	-	-	-
E5	-3.02	-19.47	65.8	-	-	-	-	-	-
E6	-2.91	-34.38	66.1	-	-	-	-	-	-
E7	-3.13	-30.90	66.1	-	-	-	-	-	-
E8	-3.17	-26.97	65.9	-	-	-	-	-	-
E9	-3.49	-31.61	66.2	-	-	-	-	-	-
E10	-3.08	-26.15	66.2	-	-	-	-	-	-
E11	-3.20	-32.09	65.6	-	-	-	-	-	-
E12	-3.19	-27.4	66.3	-	-	-	8.376	43.047	226.018
E13	-3.35	-19.12	66.1	-	-	-	-	-	-
E14	-3.12	-22.11	65.6	-	-	-	-	-	-
E15	-3.17	-17.27	66.1	-	-	-	-	-	-
E16	-3.05	-30.40	65.6	-	-	-	-	-	-
E17	-2.86	-20.47	66.1	-	-	-	-	-	-
E18	-2.87	-25.85	66.1	-	-	-	-	-	-
E19	-2.90	-25.06	65.9	-	-	-	-	-	-
E20	-2.98	-28.47	66.1	-	-	-	8.68	40.62	74.01
D R1 SLM	-33.62	-20.16	136.2	-	-	-	11.53	63.64	131.76
D U2 SLM	-53.90	-15.26	116.7	-	-	-	-	-	-
D B3 SLM	-	-	-	-	-	-	-	-	-
D L4 SLM	-	-	-	-	-	-	-	-	-
D C5 SLM	-30.65	-26.18	133	-	-	-	10.28	47.44	238.74
E U1 SLM	-13.11	-28.92	67.3	-	-	-	-	-	-
E R2 SLM	-10.91	-29.22	67.3	-	-	-	5.77	43.90	118.33
E C3 SLM	-	-	-	-	-	-	9.60	91.71	172.37
E B4 SLM	-	-	-	16.70	109.53	19.81	15.42	102.99	-
E L5 SLM	-10.86	-20.92	67.1	-	-	-	-	-	-

DEPARTMENT OF SOME SUBJECT OR TECHNOLOGY
CHALMERS UNIVERSITY OF TECHNOLOGY
Gothenburg, Sweden
www.chalmers.se

CHALMERS
UNIVERSITY OF TECHNOLOGY